
Structures of Cytochrome P450 Enzymes

1

Thomas L. Poulos and Eric F. Johnson

1.1 Introduction

The first cytochrome P450 structure, P450cam or CYP101A1, was solved in the early 1980s [1, 2], followed by the second, P450BM3, in 1993 [3]. At the time of the 3rd edition of this book published in 2004, there were a total of 13 unique P450 crystal structures deposited in the Protein Data Bank (PDB). As of April 2014, the PDB lists 449 entries with the name P450 in the title and of these about 54 are unique structures. The many new structures solved since the 3rd edition include various substrate/ligand complexes, P450s in various conformational states, and a few new P450-redox protein complexes. This wealth of new structural information has been particularly useful in a better understanding of P450 dynamics and how the P450 active site adapts to substrates of diverse sizes and shapes.

T. L. Poulos (✉)
Departments of Molecular Biology and Biochemistry,
Pharmaceutical Sciences, and Chemistry, 2206 Natural
Sciences 1, Mail Code 3900, University of California,
Irvine, CA 92697-3900, USA
e-mail: poulos@uci.edu

E. F. Johnson
Department of Molecular and Experimental Medicine,
The Scripps Research Institute, 10550N, Torrey Pines
Rd., La Jolla, CA 92037-1000, USA
e-mail: johnson@scripps.edu

1.2 Overall Architecture

There now are a sufficient number of structures to safely state that the overall P450-fold is quite conservative. While it remains the case that there are no nonheme proteins that exhibit the P450-fold, there now are a small handful of examples of enzymes that exhibit the P450-fold but do not catalyze traditional P450 chemistry. These include the NO reductase, P450nor [4, 5], prostacyclin synthase [6–8], allene oxide synthase [8–11], P450BS β [12], and a related peroxygenase, CYP152L1 [13], which hydroxylates fatty acids but does so using H₂O₂ as the oxidant.

The structures of six P450s are shown in Fig. 1.1, while Fig. 1.2 highlights some of the key secondary structural elements. Although the overall fold is maintained, the precise positioning of various structural elements differs substantially. In general, the closer to the heme, the more conserved the structure, especially helices I and L, which directly contact the heme. As expected, those regions controlling substrate specificity differ the most, especially the B' helix. For example, in P450eryF, the B' helix is oriented about 90° from the orientation observed in P450cam. The effect is a substantial change in local environment, which is required for substrate selectivity.

Not too surprisingly, the most conserved elements of the P450 structure center on the heme-thiolate oxygen activation chemistry. The most noteworthy is the β -bulge segment housing the Cys ligand (Fig. 1.3), just prior to the L helix. This rigid architecture is required to both protect

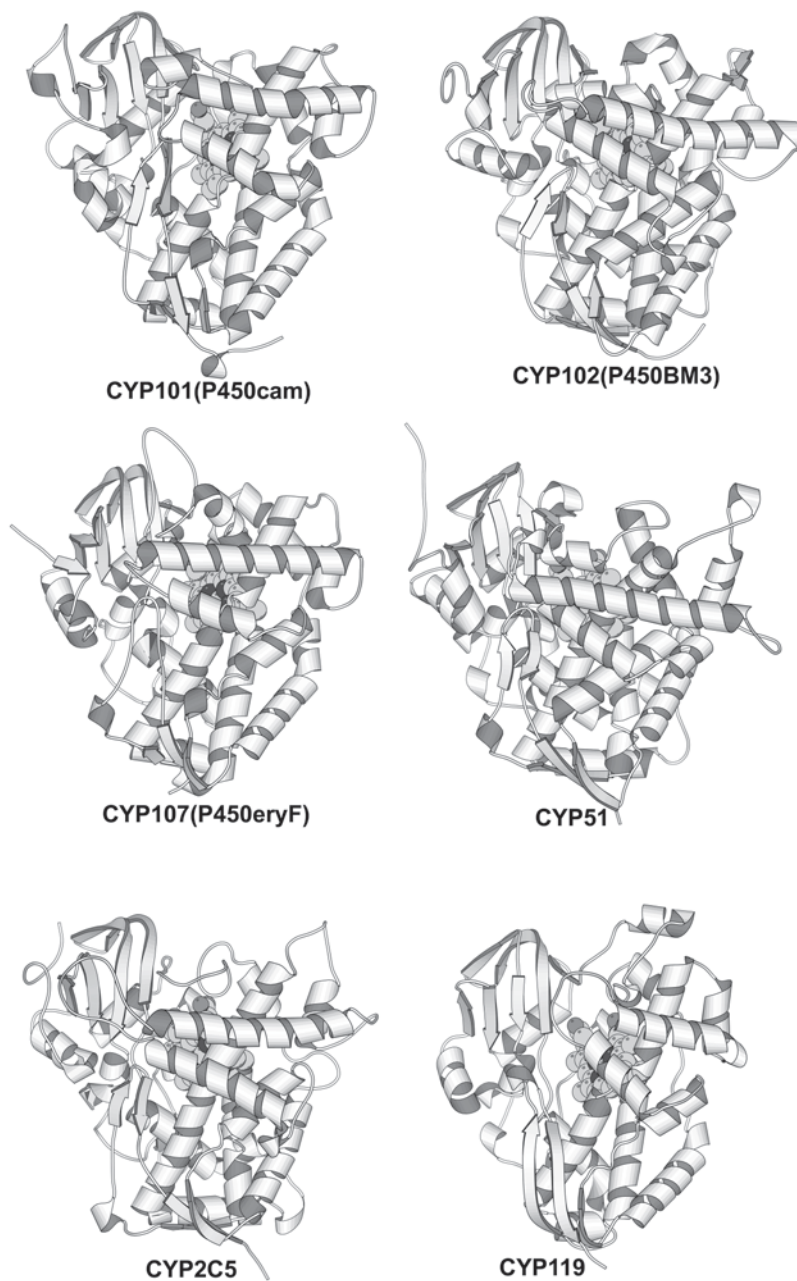


Fig. 1.1 A representative example of known P450 structures illustrating the common three-dimensional fold

that Cys ligand and hold it in place in order to be within H-bonding distances of two peptide NH groups, although the H-bonding geometry is good for only one H-bond. This arrangement is not only found in all P450s but also in two closely related enzymes, nitric oxide synthase (NOS)

and chloroperoxidase (CPO). Both NOS and CPO are heme–thiolate enzymes that, like P450s, catalyze monooxygenation reactions. Like P450, the Cys ligand in CPO is near peptide bond NH groups [14]. NOS is similar, except that an H-bond is provided by the indole ring N atom of a

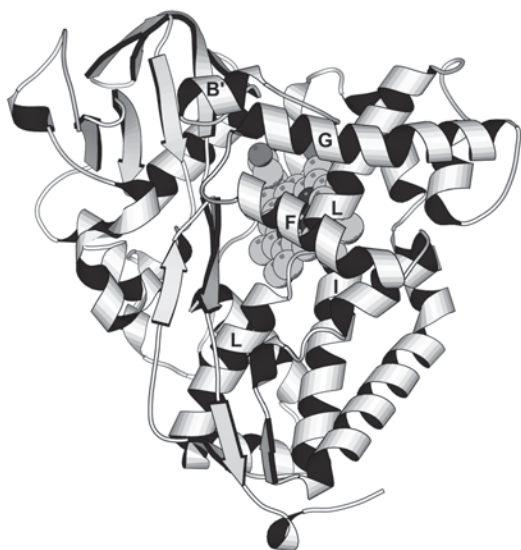


Fig. 1.2 The structure of P450cam (PDB: 5CP4) with key helical segments labeled. *PDB Protein Data Bank*

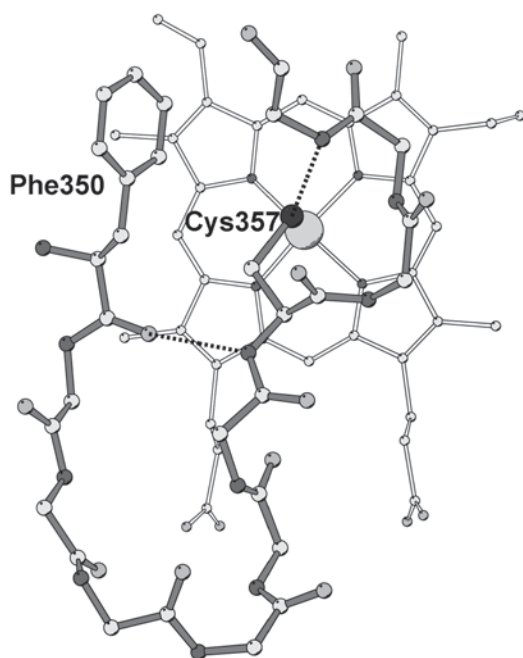


Fig. 1.3 The Cys ligand “loop” in P450cam. The *dashed lines* indicate key hydrogen bonding interactions that aid in stabilizing the Cys ligand. *Cys* cysteine

conserved Trp residue [15–17]. Such an H-bonding arrangement is not unique to heme–thiolate proteins, but is a characteristic feature of proteins

containing Cys–Fe ligation, and was first observed in the ferredoxins [18]. These H-bonds aid in regulating the heme iron redox potential [19, 20]. Without such H-bonds, the redox potential would be too low for reduction by redox partners. Thus, it appears that the protein must provide a suitable electrostatic environment around the Cys ligand in order to maintain the redox potential in a physiologically accessible range. The same is true for a close cousin to P450, the peroxidases. Here histidine (His) serves as the axial ligand, but, in this case, it is necessary to increase rather than decrease the redox potential [21]. As a result, the His ligand H-bonds with a buried Asp residue that imparts greater imidazolate character to the His, thus lowering the heme iron redox potential [22–26].

The other highly conserved region involved in O₂ activation is the portion of helix I near the heme Fe (Fig. 1.4). Thr252 is involved in a local helical distortion in P450cam such that the threonine (Thr) side-chain OH donates an H-bond to a peptide carbonyl oxygen that would normally be involved in an α -helical H-bond. This Thr is not strictly conserved. For example, P450eryF contains an Ala instead of a Thr [27] and P450cin has an Asn [28]. Even so, these outliers also exhibit a similar distortion in the I helix. This arrangement is thought to be quite important for the proper delivery of protons to the iron-linked oxygen required for cleavage of the O–O bond, thus generating the active Fe–O hydroxylating species. The growing consensus is that ordered solvent at the active site serves as the direct proton donor to the iron-linked dioxygen [29–32]. P450–oxy complexes tend to be rather unstable, which is why there are only two crystal structures of P450–oxy complexes: P450cam [31, 33] and P450eryF [34]. In the P450cam–oxy complex, the I helix opens up slightly which provides sufficient room for two new waters to move into the active site. These waters form an H-bonded network that is thought to be important for the proper delivery of protons to dioxygen in order to promote heterolytic cleavage of the O–O bond (Fig. 1.4). While the positioning of new waters in the active site requires changes in the I helix, there are no changes in the P450eryF–oxy complex except

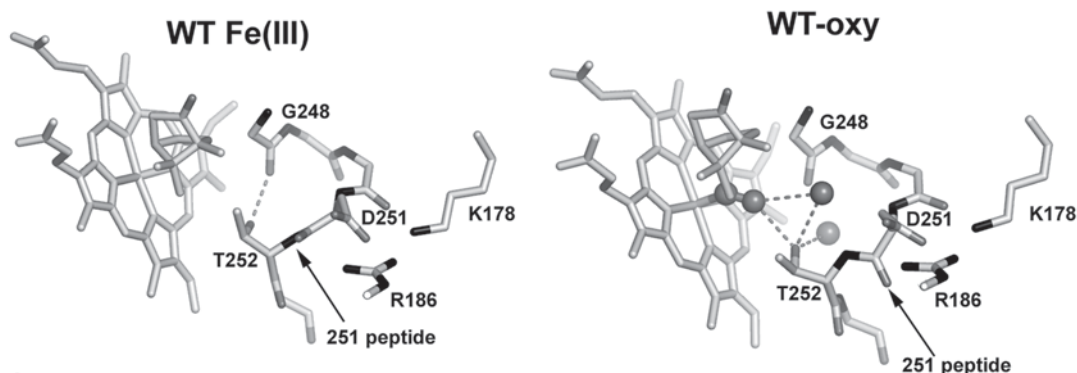


Fig. 1.4 A comparison of the I helix region in ferric and oxy-P450cam (PDB: 2A1M). When O_2 binds, the I helix opens up and the H-bond between Thr252 and Glu248 is

broken. This opening enables additional waters to move into the active site that are thought to be critical for completing a protein relay network required for O_2 activation

for the repositioning of a water molecule. Since the conserved Thr252 found in P450cam is replaced by Ala in P450eryF (Fig. 1.5), the I helix is already in an open conformation similar to that of P450cam-oxy. It appears that P450eryF uses a substrate-assisted mechanism [35] since a substrate OH anchors the key water in place via H-bonding and is essential for activity. While the details of the proton shuttle machinery may differ from one P450 to the next, the surrounding protein groups and, in at least one case, the substrate, generally position solvent in the active site for

proton delivery to dioxygen resulting in cleavage of the O–O bond.

1.3 Structural Features for Membrane Binding

In contrast to prokaryotic P450s, eukaryotic P450s are generally membrane-bound proteins. Most eukaryotic P450s are incorporated into the endoplasmic reticulum. However, several mammalian P450s that participate in the synthesis of

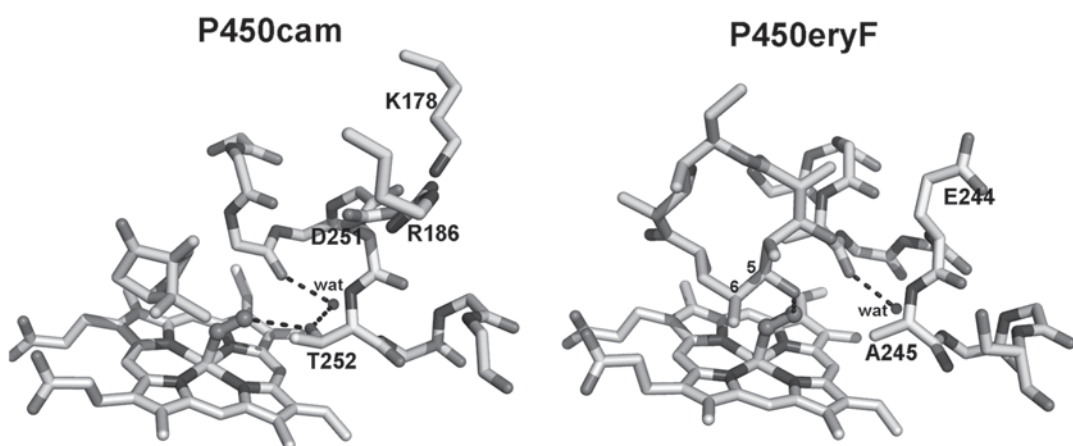


Fig. 1.5 A comparison of the solvent-mediated hydrogen bonding network in oxy-P450eryF (PDB: 1Z8O) and the oxy complex of P450cam. Unlike in P450cam, there is very little movement of the I helix in P450eryF when O_2

binds. This is probably because Thr252 in P450cam is replaced by Ala245 in P450eryF. As a result, the I helix is already more open in P450eryF

sterols, steroids, and bile acids are located on the matrix side of the mitochondrial inner membrane. A longer N-terminal polypeptide chain of roughly 30–50 amino acids precedes the catalytic domain in eukaryotic P450s and mediates membrane targeting. In the case of mitochondrial P450s, the targeting sequences are cleaved during import of the protein into the mitochondrion [36]. In contrast, the leader sequences of microsomal P450s are retained and inserted into the endoplasmic reticulum during protein synthesis [37]. The insertion process stops at the end of a hydrophobic stretch of roughly 20 amino acid residues, which are likely to form a helix in order to reduce the energetic costs of placing the polar peptide backbone in the nonpolar core of the bilayer [38]. A short linker region of about ten amino acids, which often includes positively charged amino acid residues, connects the transmembrane helix (TMH) to a generally conserved proline at the N-terminus of the structurally conserved P450-fold. The length of the 20 amino acid TMH corresponds roughly to the 3-nm width of the hydrocarbon core of the bilayer [39]. Additionally, the polar head groups of the phospholipids add another 1 nm outer layer on each side of the hydrophobic core, suggesting that a portion of the linker region resides in the polar head group layer.

The TMH is not required for function, as illustrated by the expression and successful reconstitution of several P450 monooxygenases in which this region was deleted [40–44]. Almost all of the currently available crystal structures have been determined for microsomal P450s expressed and crystallized without the TMH [45]. Initial structures of the human aromatase, CYP19A1, are an exception. Although the full-length aromatase was crystallized, the TMH and linker regions were disordered in the crystal [46]. Subsequently, engineered mutants of aromatase were expressed in *Escherichia coli* without the TMH, and these structures were not significantly affected by the absence of TMH [47].

Recently, additional evidence for the helical nature of the TMH was obtained from solid-state nuclear magnetic resonance (NMR) studies of rabbit microsomal CYP2B4 incorporated

into magnetically oriented bicelles [48] and from a crystal structure reported for full-length, *Saccharomyces cerevisiae* CYP51A1, a sterol 14 α -demethylase [49]. This crystal structure includes the linker region, TMH, and an additional amphipathic helix at the N-terminus. Interactions of the latter with a neighboring molecule in the crystal lattice contributed to a well-ordered N-terminus for structure determination. As a result, the predicted helical secondary structure of the TMH was confirmed, and a role for the additional amphipathic N-terminal helix in membrane binding to the distal leaflet of the bilayer was proposed, as illustrated in Fig. 1.6. Although the N-terminal amphipathic helix is not a general feature of microsomal P450s, this structure suggests that some P450s with extended N-terminal sequences could exhibit additional membrane interactions with the distal leaflet of the bilayer. In the *S. cerevisiae* CYP51A1 structure, the C-terminal end of the 24-residue TMH lies along the surface of the catalytic domain and passes from the proximal face to the distal face of the P450 along a trajectory that is roughly parallel with β -sheet 1, Fig. 1.6. The C-terminal end of the TMH helix corresponds to the linker region and is amphipathic with polar residues exhibiting hydrogen-bonding interactions with the catalytic domain and hydrophobic residues on the outer surface. This suggests that the observed trajectory is likely to be maintained when the enzyme is bound to the membrane [49]. As depicted in Fig. 1.6, a portion of the catalytic domain is likely to protrude into the membrane when the TMH resides in the lipid core. The surface of the catalytic domain surrounding this region is relatively hydrophobic for CYP51A1 (Fig. 1.7) as well as other membrane P450s [45, 50], which is likely to facilitate interactions with the lipid core of the bilayer.

This hydrophobic surface is formed by the N-terminal portion of the catalytic domain together with the helix F–G region, and there are distinctive structural differences between mammalian P450s and soluble prokaryotic P450s for this portion of the catalytic domain. The initial comparison of the first structure of a microsomal P450, CYP2C5, with structures of CYP102 and

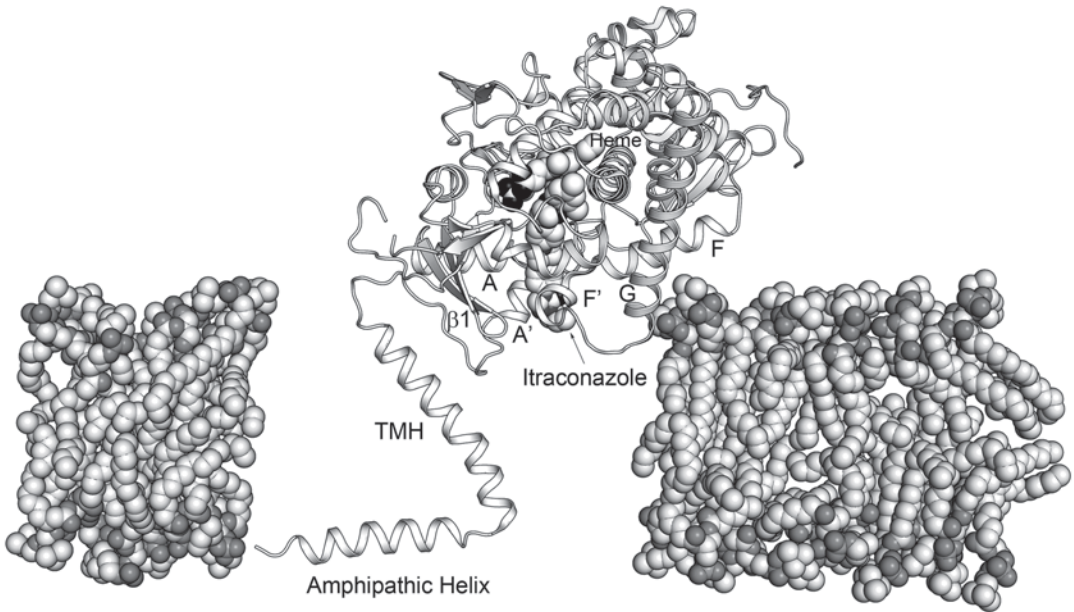


Fig. 1.6 Hypothetical model for the membrane binding of microsomal P450s. The cartoon depicts the experimentally determined fold of full-length, *Saccharomyces cerevisiae* CYP51A1 (PDB: 4KOF). For reference, the structure of the TMH is flanked by modeled arrays of phospholipid molecules depicted as CPK atoms. The amphipathic N-terminal helix is positioned at the transition

of the polar head group and the hydrophobic layers with its hydrophobic surface oriented toward the lipid layer. The heme and bound inhibitor, itraconazole, are also rendered as CPK atoms. Itraconazole passes out of the access channel between helices A' and F', which are oriented toward the lipid portion of the bilayer. *TMH* transmembrane helix

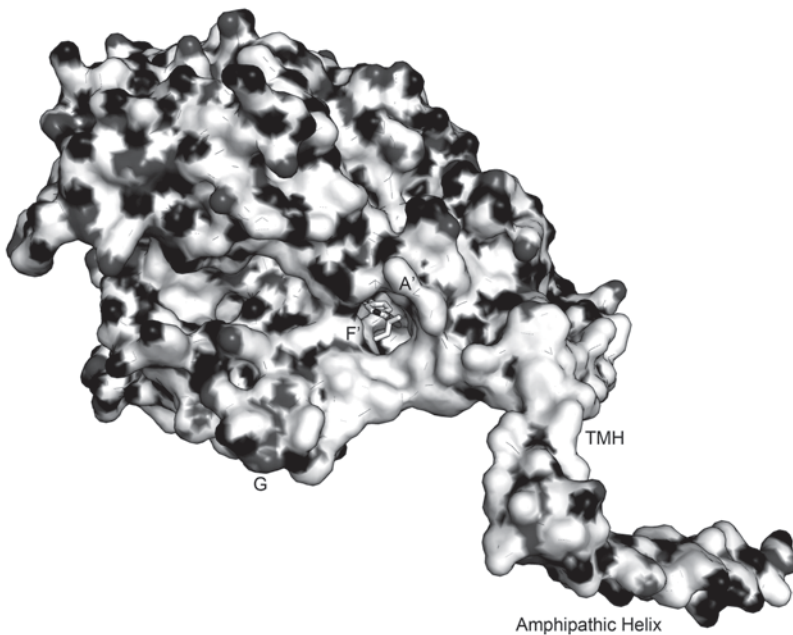


Fig. 1.7 Surface rendering of full-length, *Saccharomyces cerevisiae* CYP51A1, (PDB: 4KOF) with acidic and basic residues colored *black* and *gray*, respectively. Note the relative absence of charged residues on the surface of the catalytic

domain surrounding the entrance channel and the TMH. Itraconazole is depicted as a stick figure in the entrance channel. The hydrophobic surface surrounding the entrance channel is oriented toward the membrane in Fig. 1.6. *efj*1

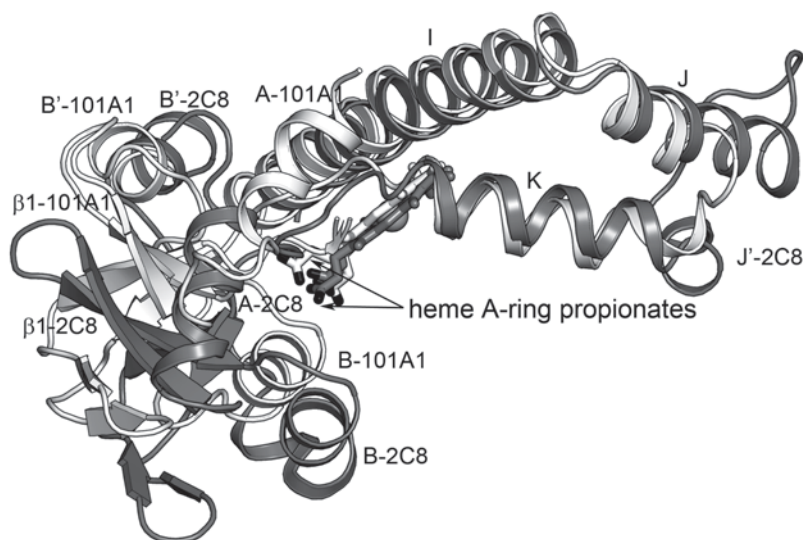


Fig. 1.8 Superposition of CYP101A1 (*light gray*) and CYP2C8 (*dark gray*). The hemes are shown as stick figures with oxygen atoms colored black. The heme iron is depicted by a *sphere*. Although helices *I* through *K* su-

perimpose well, the N-terminal region is shifted outward for CYP2C8 relative CYP101. Different orientations are evident for the heme A-ring propionates

CYP101 [50, 51] indicated that the N-terminal portion of the catalytic domain from the linker region and to the helix B–C loop of CYP2C5 is shifted significantly toward the proximal face when compared to structures of prokaryotic P450s (Fig. 1.8). The generality of this observation was established by a retrospective analysis of a larger number of structures from diverse eukaryotic and soluble prokaryotic P450s by Denisov et al. [52]. As a result of this shift in position, the heme A-ring propionate is oriented toward the proximal side of the heme plane in most mammalian membrane P450s, where it often interacts with basic amino acid side chains. Notable exceptions are eukaryotic CYP51A1 and the non-monoxygenases, CYP8A1, a prostacyclin synthase and CYP74A1, a plant allene oxide synthetase. The heme A-ring propionate resides more typically on the distal side of the heme plane in prokaryotic P450s, with some exceptions. This shifted N-terminal/ β -sheet domain resides near the connector between helices F and G, which is typically longer in eukaryotic P450s than in soluble, prokaryotic P450s. The structure of the F–G helical region varies extensively between mammalian P450s and often exhibits two

short helices, F' and G'. Together these elements form the hydrophobic surface near the N-terminus of the catalytic domain that is likely to be inserted into the membrane [45, 50].

The orientation of the hydrophobic surface toward the membrane is supported by studies indicating that antibody epitopes in this region are inaccessible to the antibody when CYP2B4 is in its native membrane [53], whereas epitopes on other portions of the molecule react with their respective antibodies. These and other epitope-mapping studies indicate that extensive portions of the surfaces of drug-metabolizing P450s are accessible to the antibodies when bound to membranes, as shown in Fig. 1.9 and reviewed in more detail [54]. Atomic force microscopy experiments estimate that the height of microsomal CYP2B4 above a model phospholipid membrane is roughly 35–45 nm [55]. This would require a portion of the protein to be buried in the membrane, which is likely to be the hydrophobic region near the N-terminus of the catalytic domain. Additionally, studies of the association of CYP2B4 with Langmuir–Blodgett phospholipid monolayers indicate that the protein displaces an area that is larger than a single TMH [56]. This

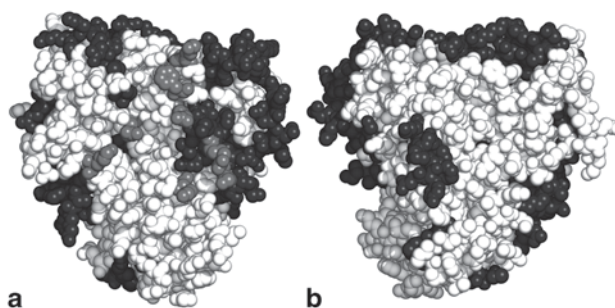


Fig. 1.9 CPK rendering of the proximal (a) and distal surfaces (b) of CYP2C5 (PDB: 1N6B). Antibody epitopes recognized when the P450s are bound to microsomal membranes are colored *dark gray*, as reviewed [54]. Several conserved amino acid side chains that have been implicated in P450 reductase interactions with CYP2B4

[156] are colored *medium gray*. The orientation of the protein is similar to that depicted in Fig. 1.6 efj-1 with the N-terminus of the catalytic domain positioned toward the *bottom* of the figure. (Reproduced from *Cytochrome P450, Third Edition* with permission from Springer Science+Business Media)

result would be consistent with the penetration of the hydrophobic surface of the protein into the adjacent leaflet of the lipid bilayer.

Molecular dynamics (MD) simulations of the binding of human microsomal P450s with phospholipid bilayers, reported initially for CYP2C9 [57–59] and CYP3A4 [52, 60], observed stable binding orientations for the catalytic domains with the hydrophobic surface of the catalytic domain immersed in the proximal leaflet of the phospholipid bilayer, Fig. 1.10. The structure of the catalytic domain was reported to be stable and exhibiting dynamic motion with root-mean-square deviation (RMSD) values of less than 2.5 Å from the starting structures.

The maximum heights of the catalytic domains above the membrane surface in these MD simulations are similar to that of 35–45 nm determined by atomic force microscopy for CYP2B4 [55]. Additionally, the tilt of the heme plane relative to the membrane normal, Fig. 1.10, in the models of membrane-binding interactions can be compared to results from biophysical studies for this angle. This tilt angle has been estimated for CYP17A1 and CYP21A2 based on the anisotropic decay of the absorption spectrum following photodissociation of carbon monoxide complexes by polarized light. This approach gives two solutions for the angle of the orientation of the heme plane relative to the membrane normal of either 43° or 27° and 52° or 12°, respectively for

the two enzymes [61]. The larger values are similar to a single value for tilt angle of $59.7 \pm 4.1^\circ$ estimated from the dichroic ratio observed for the absorption of visible light by the heme chromophore of P450 3A4 bound to nanodisc membranes. Tilt angles for the heme in the initial MD simulations for P450 2C9 were reported to be $55 \pm 5^\circ$ [58], and in additional MD simulations for P450s 1A2, 2A6, 2C9, 2D6, 2E1, and 3A4, using similar conditions, the heme-tilt angles differed between P450s and ranged from $56 \pm 5^\circ$ for CYP3A4 to $72 \pm 6^\circ$ for CYP2D6 [59]. Differences between P450s are not unexpected, as the distal surfaces of microsomal P450s differ significantly, and these differences are likely to affect the angle tilt and extent of membrane insertion.

Heme-tilt angles observed for CYP3A4 in MD simulations from two different studies were reported to be 68.7° – 75.9° [60] and $56 \pm 5^\circ$ [59]. The reported differences between the two MD simulations could reflect differences in the model membranes used in the simulations, as well as different initial models for the N-terminus used in the MD simulations. As structures for the native N-terminal domains were not available for CYP3A4, and the other proteins characterized in these studies, they were modeled *de novo* with the hydrophobic portion of the N-terminus modeled as a TMH. The structure of the linker region in these proteins is less certain, and is likely to vary between P450s. X-ray crystal structures of

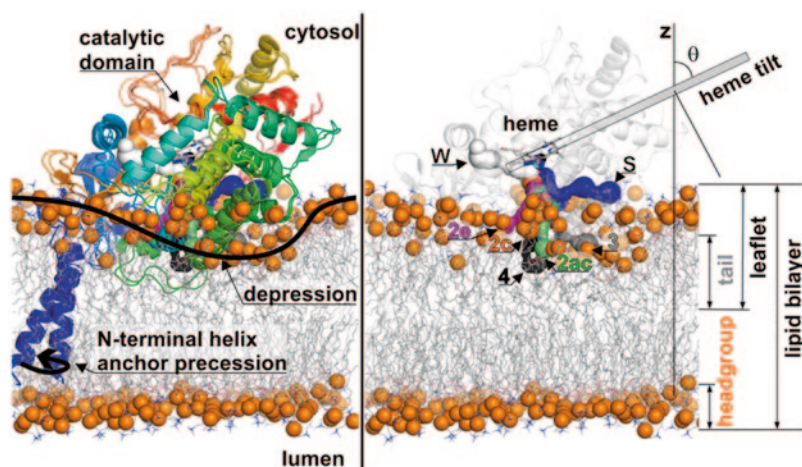


Fig. 1.10 Immersion of CYP2C9 in a dioleoylphosphatidylcholine (DOPC) lipid bilayer. (Left) Overlaid snapshots of CYP2C9 taken at 0.1 and 1 μ s molecular dynamics (MD) simulations showing that the catalytic domain is immersed in a membrane depression framed by lipid phosphate groups (shown as orange spheres). Water molecules are not shown for clarity. The N-terminal helix shows precessional movement about the bilayer normal. The fold of the catalytic domain is conserved and agrees with that observed in X-ray crystallography experiments. (Right) Snapshot taken at 1 μ s of MD simulation showing positions of active site access and egress

channels computed from the heme moiety using MOLE 2.0.20. The water channel (white) points toward the cytosolic environment, whereas solvent channel S (blue) points above the lipid head groups. All other channels point inside the bilayer. Channels 2e, 2c, and 3 point into the lipid head group region, whereas channels 4 and 2ac point below the lipid head groups. The heme tilt angle θ (between the heme plane and the bilayer normal z , i.e., defined according to Baylon et al. [60] is depicted. (Reprinted with permission from [59], copyright 2013 American Chemical Society. The channels are designated as described [93])

mammalian microsomal P450s have generally been determined for proteins without their N-terminal TMH, and, in most cases, the native linker regions of family 2 P450s were modified to correspond to the linker region of CYP2C3, as described for CYP2C5, [40, 41, 50]. Moreover, the structures of these short N-terminal regions have not been defined for many P450s. CYP3A4 is an exception [62, 63], and the native linker region exhibits an A'' helix following a turn that directs the polypeptide chain along β -sheet 1 from the N-terminus of the catalytic domain near the hydrophilic proximal face toward the hydrophobic distal surface. This trajectory is similar, but not identical, to that observed more recently for the structure of full-length *S. cerevisiae* CYP51A1, Fig. 1.6. The initial model used by Baylon et al. [60] incorporated a flexible link between helix A'' and the TMH, which provides some flexibility for the orientation of the TMH independently of the catalytic domain during the MD simulation.

The initial model used by Berka et al. [59] for the N-terminus CYP3A4 was based on their earlier equilibrated CYP2C9 model obtained following a 0.25 μ s MD simulation [58]. Interestingly, the helix A'' region and the TMH of the initial model of P450 2C9 were built as a continuous helix, but a kink developed between helix A'' region and the TMH during the MD simulation that allowed the polar Arg side chains in the linker region to reside in the polar region of the bilayer, and the TMH to span the lipid core of the membrane, as illustrated in Fig. 1.10 by a 1 μ s equilibrated model from a later study [59]. Helix A'' may not be a generally conserved feature for linker regions, as the same segment of the native linker regions does not exhibit an A'' helix in the structure of human CYP1A2 [64], and is not evident in the MD simulation model of CYP1A2 [59]. Both CYP1A2 and CYP3A4 exhibit short N-terminal helices that are roughly orthogonal to the TMH and that are positioned at the interface between

the polar head group and lipid layers of the distal leaflet of the bilayer in the MD simulations of Berka et al. [59]. These models are similar to the bimodal membrane binding proposed for full-length *S. cerevisiae* CYP51A1 [49].

Although the MD simulations generally support the notion that a portion of the distal surface is embedded in the membrane surface, the results of biophysical experiments and topology studies often show differences that are difficult to reconcile with a single model. Fluorescent quenching of tryptophan residues introduced on the surface of CYP2C2 by site-directed mutagenesis suggested that residues 36 and 69 flanking helix A and 380 in β -sheet 2 of CYP2C2 are inserted into the fatty acyl core of the bilayer, while residue 80 on helix B and 225 at the turn between helices F' and G' are in the polar region of the phospholipid bilayer [65], leading the authors to propose a more vertical orientation for CYP2C2 than was observed in the MD simulations for the closely related CYP2C9 [57, 58]. Experimental evidence indicates that P450s are present as both monomers and dimers in membranes [66, 67], and a more vertical orientation relative to the membrane surface would be consistent with models for the dimerization of the catalytic domain of N-terminally truncated P450 2C8 in aqueous solution that involve interactions of the helix F–G loop region [63]. This model for the dimerization of 2C8 is supported by cross-linking studies for the membrane-bound full-length CYP2C8 [68]. Additionally, these cross-linking studies implicated the linker region and TMH in the dimerization of membrane-bound, full-length CYP2C8 expressed in mammalian cells or in *E. coli* membranes. Cys-scanning mutagenesis indicated that reactive cysteines reside on a single side of the TMH, whereas several consecutive residues were reactive in the linker region suggestive of a more flexible structure. This flexibility is necessary for reorientation of the proximal faces relative to TMH in order to form a P450 dimer through interactions of the helix F–G region. P450 dimerization in membranes is thought, in some cases, to inhibit reduction by the microsomal cytochrome P450 reductase, so the monomer is

likely to be the predominant functional form of the enzyme [66].

As mitochondrial P450s lack the N-terminal TMHs found in microsomal P450s, the interactions of the catalytic domain with the matrix side of the inner membrane are likely to be the predominant membrane interaction. Consistent with a role for the helix A', F', and G' regions in membrane binding, these regions exhibit nonpolar, exterior surfaces in structures of mitochondrial P450s 11A1 [69, 70], 11B1 [71], and 24A1 [72]. Moreover, substitutions of more polar residues for hydrophobic residues on the F' and G' surfaces increase salt extractability and solubility of mitochondrial P450 27A1 [73]. The helix F–G region of mitochondrial P450 11A1 is also protected from chemical modification by membrane association [74]. Similarly, microsomal P450s expressed without their TMH retain capacities to bind to phospholipid membranes, and mutations made to the helix F' and G' regions of microsomal P450s 2C5 [41], 2D6 [75], and 7A1 [76] facilitate extraction in high salt buffers. These observations suggest the extended loop between helices F and G in eukaryotic P450s contributes to membrane binding for both mitochondrial and microsomal P450s.

1.4 Conformational Dynamics for Substrate Access

Many P450 structures are in the so-called closed state with no obvious way that substrates can gain access to the active site. As a result, substrate entry and product egress may involve rather large conformational changes. Once the P450cam structure became available, an immediate puzzle was how camphor gains access to the active site since the substrate is buried, and there is no obvious opening. The substrate-free and bound structures showed no differences, although substrate-free P450cam exhibited higher thermal motion in the B', F, and G helices, suggesting that these regions must move to allow substrate to enter the active site [77]. The first clear indication that conformational changes are important in substrate binding was the struc-

ture of palmitoleic acid bound to P450BM3 [78], which was followed by a higher-resolution structure [79]. Interestingly, the experimentally observed conformational change was correctly predicted based on computational methods [80, 81] before the substrate-bound crystal structure was solved. The main motion involves the F and G helices sliding over the surface of the I helix. This motion closes off the entry channel, indicating that substrates enter near the F/G loop region that is similar to that of P450cam.

There now are a handful of P450 structures in the open and closed forms and in all of them, the F and G helices and the F/G loop undergo large changes. Not surprisingly, the most extensive analysis has been with P450cam. In the open form [82], the F and G helices move, and the B' helix region becomes disordered. It also has been possible to trap the P450cam access channel using a series of tethered compounds where the substrate is attached to a long linker that extends out of the active site [83, 84]. A principal component analysis of 30 different tethered compound structures indicates that there are three dominant conformational states available to P450cam: closed, partially open, and fully open [84].

Two close homologues to P450cam with about 46% sequence identity with P450cam, CYP101D1 [85] and CYP101D2 [86], have now been characterized. Both catalyze exactly the same reaction as P450cam, but there are substantial differences with respect to the open and closed states and the relationship between spin-state and substrate binding. For example, CYP101D2 has been crystallized only in the open state, but camphor can be soaked into the crystals and binds in the active site [86]. The camphor, however, does not bind in a productive mode, but instead the carbonyl O atom of the substrate H-bonds with the water coordinated to the heme iron (Fig. 1.11). MD simulations of CYP101D2 show that this P450 can adopt various conformational states, mainly by motions of the F/G helical substrate access channel, and provides a dynamic picture of substrate binding consistent with other P450s [87]. Perhaps the most unexpected difference between P450cam and its close cousins is that camphor binding to CYP101D1

gives only about 40% high spin even with excess substrate. In addition, the Fe₂S₂ ferredoxin that supports CYP101D1 catalysis, Arx, is able to reduce substrate-free 100% low-spin CYP101D1, while only high-spin substrate-bound P450cam can be reduced by its redox partner, Pdx. In addition, Pdx can support CYP101D1 catalysis, while only Pdx can support P450cam catalysis [88]. There is nothing obvious in the structures that can explain these differences other than the fact that in CYP101D2 the substrate can bind to the low-spin open state, albeit in a nonproductive binding mode (Fig. 1.11). One simple way of rationalizing these differences is to hypothesize that CYP101D1 can bind camphor in various orientations that are consistent with a water molecule remaining coordinated to the heme iron, as in CYP101D2, thus giving a substrate-bound mostly low-spin complex. Upon reduction of the heme iron, the water ligand is displaced and the substrate can “relax” to a productive binding mode. This hypothesis requires that CYP101D1 is “looser” than P450cam and can more readily adopt the open conformation. The static X-ray structures do not reveal anything obvious to support this scenario, and proof one way or the other must await other approaches more in tune with measuring dynamic differences.

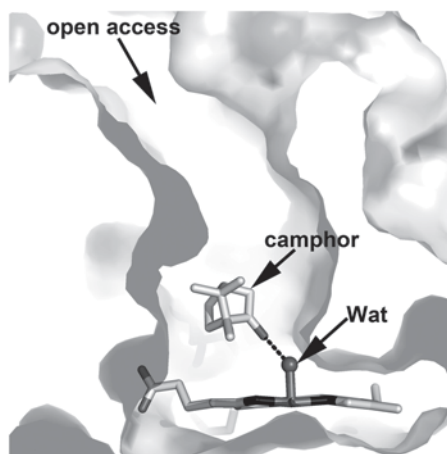


Fig. 1.11 The open substrate-binding channel in CYP101D2 (PDB: 3NV6) [86]. The substrate camphor binds but is not oriented in the productive binding mode. Instead, the camphor carbonyl O atom H-bonds with the water coordinated to the iron

1.5 Substrate Access to Membrane P450s

Similar to prokaryotic P450s, membrane P450s have been crystallized in both open and closed conformations. For example, rabbit microsomal CYP2B4 and human CYP2B6 have been crystallized in closed forms, as illustrated in Fig. 1.12, by a CYP2B6 4-(4-chlorophenyl)-imidazole complex [89] and in open forms, as illustrated by a complex of CYP2B6 with one molecule of amlodipine coordinated to the heme iron and a second molecule bound in the entry channel and protruding between helix F' and A' [90]. These two conformations of CYP2B6 differ in the positions of the helices A', A, B', F, F', and G. Open forms of rabbit CYP2B4 have also been determined where the helix F'–G' and helix B–C regions are displaced to a much greater extent by ligand and detergent interactions [91, 92]. Mammalian drug-metabolizing enzymes such as CYP2B4 bind a wide-range of compounds, and conformational changes are often associated with the capacities of these enzymes to facilitate the metabolic clearance of many compounds by accommodating large compounds in an open ac-

cess channel [45]. Mitochondrial P450s also exhibit open and closed structures. CYP11A1 and CYP11B1 exhibit closed structures for substrate complexes with the helix F and F' region blocking the substrate access channel described earlier for CYP101, Fig. 1.13. In contrast, mitochondrial CYP24A1 was crystallized in an open conformation with a large cleft between helices A' and helices F'–G'. As discussed in the previous section, these helices are likely to bind to the membrane, and the hydrophobic substrates cholesterol and vitamin D₃, respectively, could enter each enzyme from the membrane. Most P450 substrates exhibit partition coefficients that favor the hydrophobic environment of the bilayer over the aqueous phase, which suggests that the concentration of substrate in the membrane may be higher than in solution under physiological conditions.

Structures obtained with bound ligands are often closed, and substrate access channels remain closed during MD simulations that are of short duration compared to substrate dissociation rates. Nevertheless, a number of solvent channels have been identified in X-ray crystal structures and during MD simulations in an aqueous medium for soluble and truncated membrane P450s

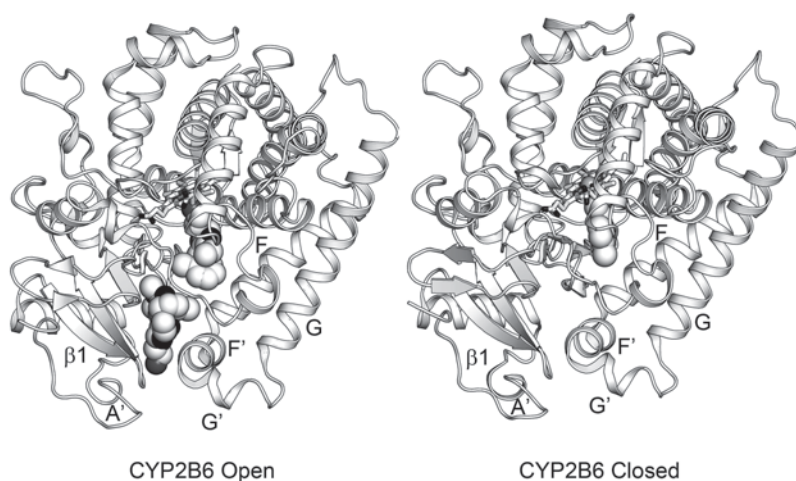


Fig. 1.12 Open (PDB: 3UA5) and closed (PDB: 3IBD) conformations of human CYP2B6. The open structure has two molecules of amlodipine (*spheres*) with one molecule of amlodipine bound to the heme iron via nitrogen coordination and the second amlodipine in the open-substrate access channel. The closed structure has one molecule of

4-(4-chlorophenyl)imidazole (*spheres*) coordinated to the heme iron with a closed substrate entrance channel. The heme is rendered as a stick figure with the iron shown as a sphere. Nitrogen and oxygen atoms are colored *light gray* and *black*, respectively

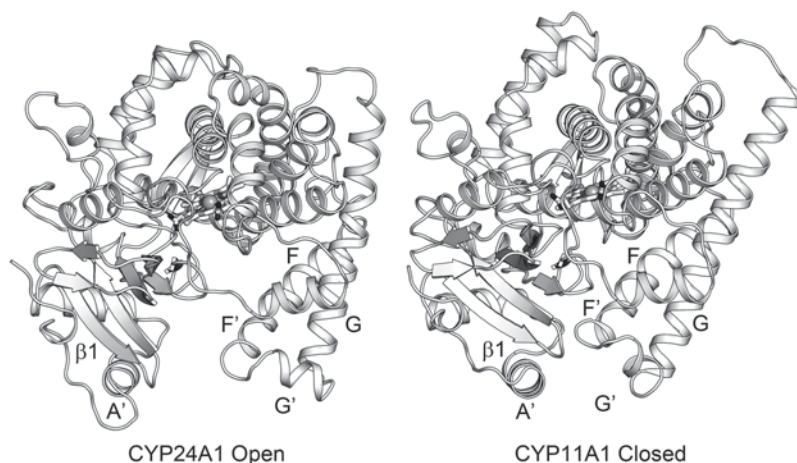


Fig. 1.13 Open (PDB: 3KNV) and closed (PDB: 3NAO) conformations of mitochondrial rat CYP24A1 and bovine CYP11A1, respectively. The heme is rendered as

a stick figure with the iron shown as a *sphere*. Nitrogen and oxygen atoms are colored *light gray* and *black*, respectively

[93]. As shown in Fig. 1.10, several of these channels are oriented into the lipid portion of the bilayer in MD simulations. Comparisons of the duration and extent of opening during MD simulations, for the catalytic domains in an aqueous environment and bound to membranes, are qualitatively similar and reveal differences in the frequency and duration of channel opening that reflect interactions between the catalytic domain and the membrane [57–60]. These solvent channels are thought to open and coalesce to form substrate access channels as seen for open conformations of soluble and membrane P450s determined by X-ray crystallography [93].

1.6 Substrate Complexes: Specific P450s

A fascinating structural feature of P450s is the ability to adapt to substrates of various sizes and shapes, yet retain the overall P450-fold and P450 electron transfer and O₂ activation chemistries. Most of our detailed understanding of protein–substrate interactions derives from highly specific P450s that bind their respective substrates tightly and thus generate crystals that diffract well. Several substrates for various specific P450s are shown in Fig. 1.14. The size and shape

of the various substrates shown in Fig. 1.14 are sufficiently diverse that the structural basis for what controls substrate specificity can, at least in part, be understood. As expected, all substrates are situated such that the atom to be hydroxylated is within 4–5 Å of the heme iron. Thus, regio- and stereoselective hydroxylation by the Fe(IV)-O species is achieved by specific protein–substrate interactions that hold the substrate in the correct position. The exception is P450BM3. The structure of the P450BM3 heme domain with palmitoleic acid [78] and N-palmitoylglycine [79] show that the fatty acid substrate is ≈ 7 –8 Å from the iron which is too far for hydroxylation. However, NMR results indicate that the substrate moves to be within 3 Å of the iron upon reduction from Fe(III) to Fe(II) [94]. Precisely how reduction is linked to such a large repositioning of the substrate remains unknown.

P450cam and P450epoK [95] represent the two extremes of substrate size and shape. Hence, a comparison between these two structures provides some insights on which regions of the structure change most in response to the requirements of substrate specificity. The two regions that differ the most between P450epoK and P450cam are the F, G, B' helices, and the F/G loop (Fig. 1.15). The B' helix is rotated 90° in P450epoK compared to P450cam. This re-

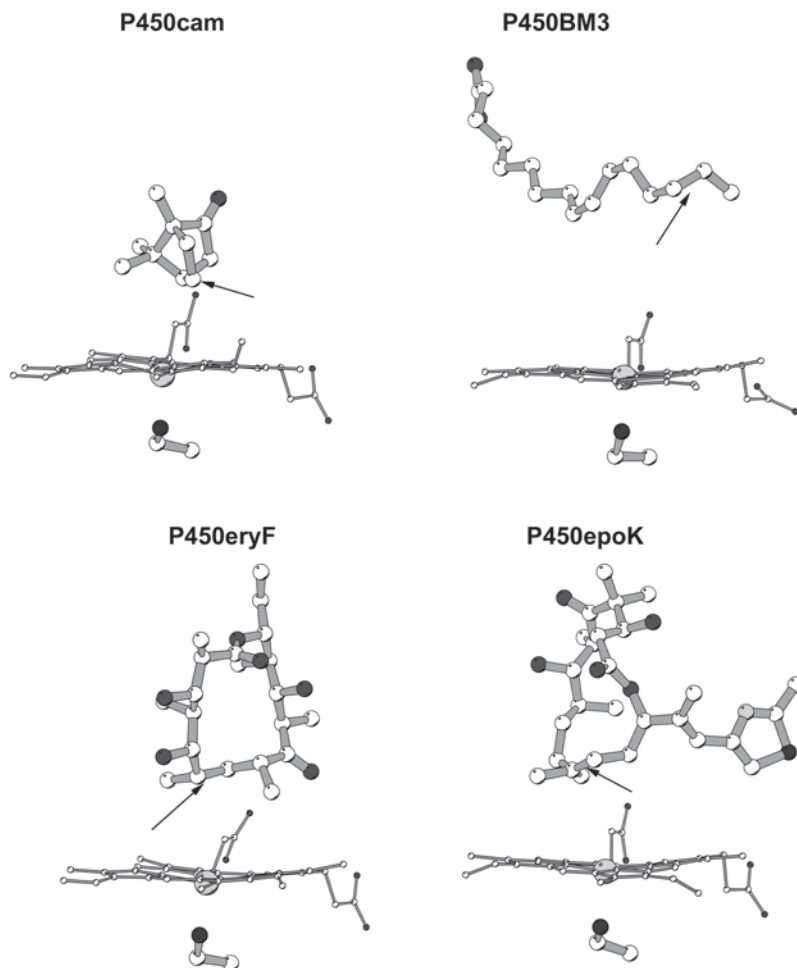


Fig. 1.14 Substrates bound to the active site of various P450s

orientation opens the substrate-binding pocket, thus making room for the thiazole ring of the substrate. The F and G helices do not superim-

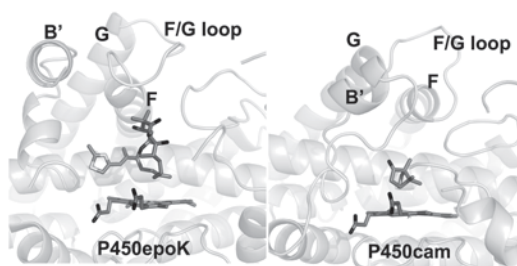


Fig. 1.15 A comparison of the P450cam and P450epoK (PDB: 1PKF) active sites. The very different size and shape of the substrates illustrate how the active site substantially differs from one P450 to the next

pose well, and the F/G loop adopts a substantially different conformation. There also are examples where a second substrate molecule is trapped in the access channel possibly because crystallization favors a partially open active site, thus leaving room for an additional molecule. Anecdotal observations not usually published show that *E. coli* “mystery” molecules will sometimes bind in the access channel or active site. This likely reflects the general hydrophobic nature of P450 active sites and the open/close dynamics that might make it possible for even specific P450s to bind different molecules present in the growth media.

An unusual example of a P450–substrate interaction is CYP107H1 (P450BioI). P450s participate in polyketide biosynthesis, and these

pathways involve multiple enzymatic steps that process a growing fatty acid-like chain into the array of complex and well-known antibiotics and other natural products. In many of these systems, an acyl carrier protein (ACP) forms a covalent bond with the substrate and transfers the substrate from one enzyme to the next. Where hydroxylation reactions are required, P450s often are involved, which means that in some of these systems the substrate is delivered to the P450 by the carrier protein. One well-characterized system is from the biotin biosynthetic pathway in *B. subtilis* [96]. P450BioI catalyzes the formation of pimelic acid through the oxidative cleavage of a fatty acid carbon–carbon bond, which then proceeds on to biotin [97, 98]. There is now a crystal structure of such fatty acid acylated ACP protein complexed with the P450 (Fig. 1.16) [99]. Structurally, P450BioI is a typical P450, yet here the substrate entry pocket has been adapted to bind ACP. Note that the substrate enters the active site near the connection between the F and G helices that is the main entry point for substrates in many P450s.

There is one final example of P450 substrate adaptability, but in this case there may be two different active sites and two enzyme activities. CYP170A1 from *Streptomyces coelicolor* catalyzes the oxidation of epi-isozizaene to an epimeric mix of 5-albaflavenol (Fig. 1.17). The structure shows that there are two substrate molecules bound, one in the expected location just above the heme and a second in the substrate access channel [100]. What was most unexpected is the finding that the conversion of farnesyl diphosphate to epi-isozizaene is catalyzed by CYP170A1. Sequence comparisons between known sesquiterpene synthase enzymes pointed toward a particular region of CYP170A1 that might be involved (arrow in Fig. 1.17). Subsequent mutagenesis in this region eliminated the synthase activity but not the P450

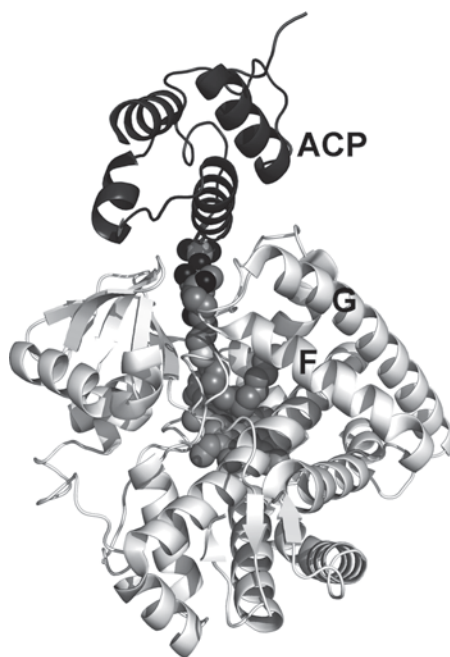


Fig. 1.16 The crystal structure of P450BioI (PDB: 3EJB) [99]. ACP (*darker* molecule) binds such that the fatty acid substrate attached to ACP extends into the active site of the P450. The opening near the F/G loop region that enables substrate entry is the same as observed in many other P450s. ACP acyl carrier protein

activity [100]. Given that we are accustomed to viewing enzymes as requiring a relatively large size to properly form the active site, it might at first seem odd that such a small region of a P450, or any enzyme, could serve a catalytic function. However, sesquiterpene synthase enzymes appear not to operate by typical acid–base catalysis requiring suitably positioned active site groups to move protons [101]. Instead, it appears that metal ions and the substrate diphosphate are the keys to catalysis and that the enzyme may serve a more passive role, providing a template for substrate and metal ion binding.

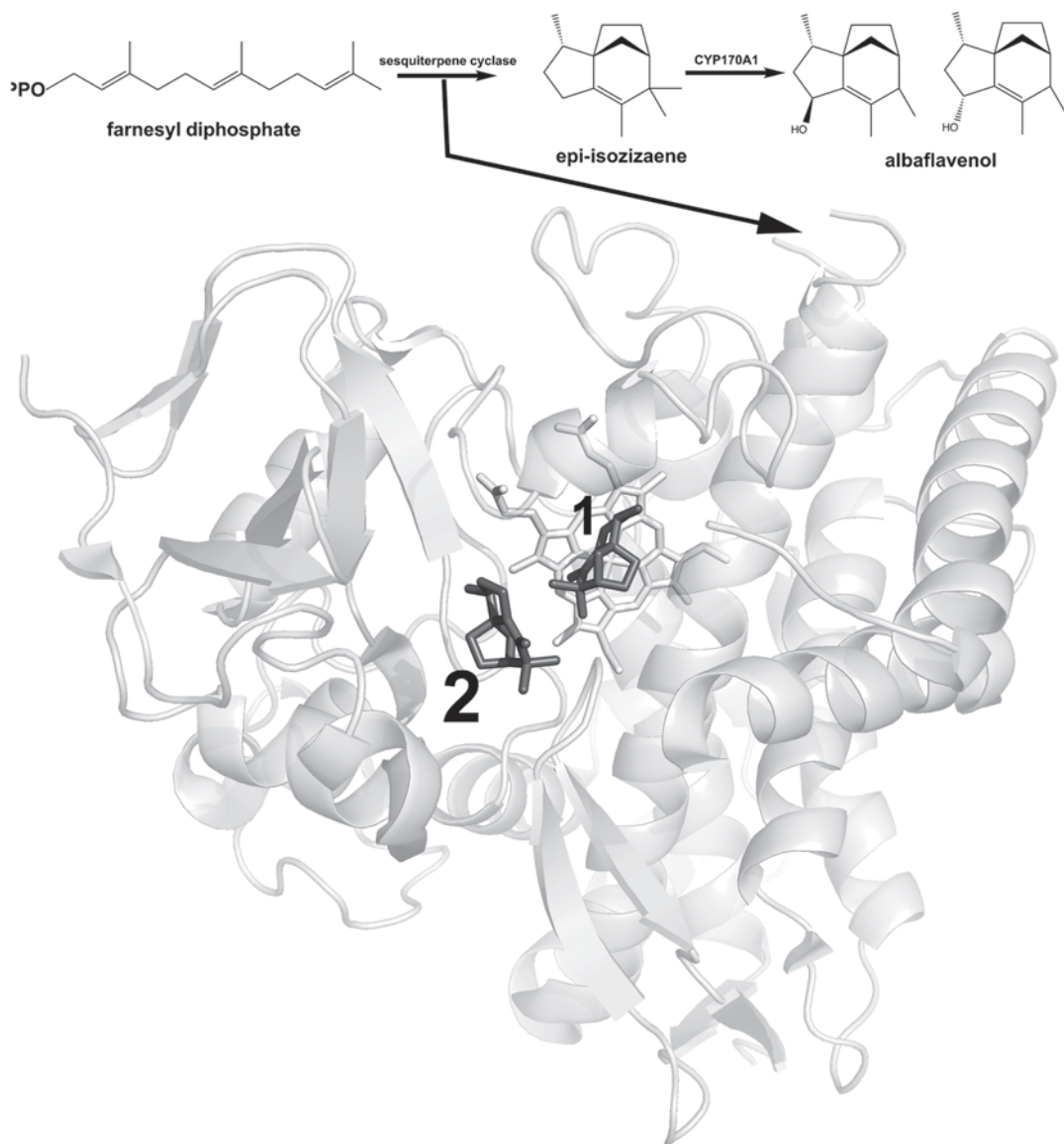


Fig. 1.17 The CYP170A1 (PDB: 3DBG) crystal structure [100] and reaction. Substrate 1 binds near the heme

as expected, while substrate molecule 2 binds in the open access channel. The site thought to be responsible for the sesquiterpene cyclase activity is indicated by the arrow

1.7 Active Site Diversity of Mammalian P450s

As with prokaryotic P450s, active site diversity underlies the unique roles of P450s in mammalian physiology. Structures now are available for several of the enzymes that hydroxylate the aliphatic side chains of cholesterol and vitamin D₃. P450 11A1 catalyzes three successive oxy-

genation reactions to produce sequentially 22*R*-hydroxycholesterol, 22*R*,20*R*-dihydroxycholesterol, and an unstable product that undergoes carbon–carbon bond scission to produce the 21-carbon steroid, pregnenolone, and isocaproaldehyde. It is thought that the peroxyanion intermediate that precedes formation of the oxene is the reactive intermediate for the third reaction [102]. The crystal structure of human mitochon-

drial CYP11A1 with cholesterol bound [70] indicates that the tetracyclic sterol moiety is bound in the entrance channel to the substrate-binding cavity under the helix F–F' region and above

β -sheet 1 with C22 of the aliphatic side chain positioned closest to the heme iron, Fig. 1.18a. Additional structures of P450 11A1 [69, 70] with the first and second products of the reaction, 22R-

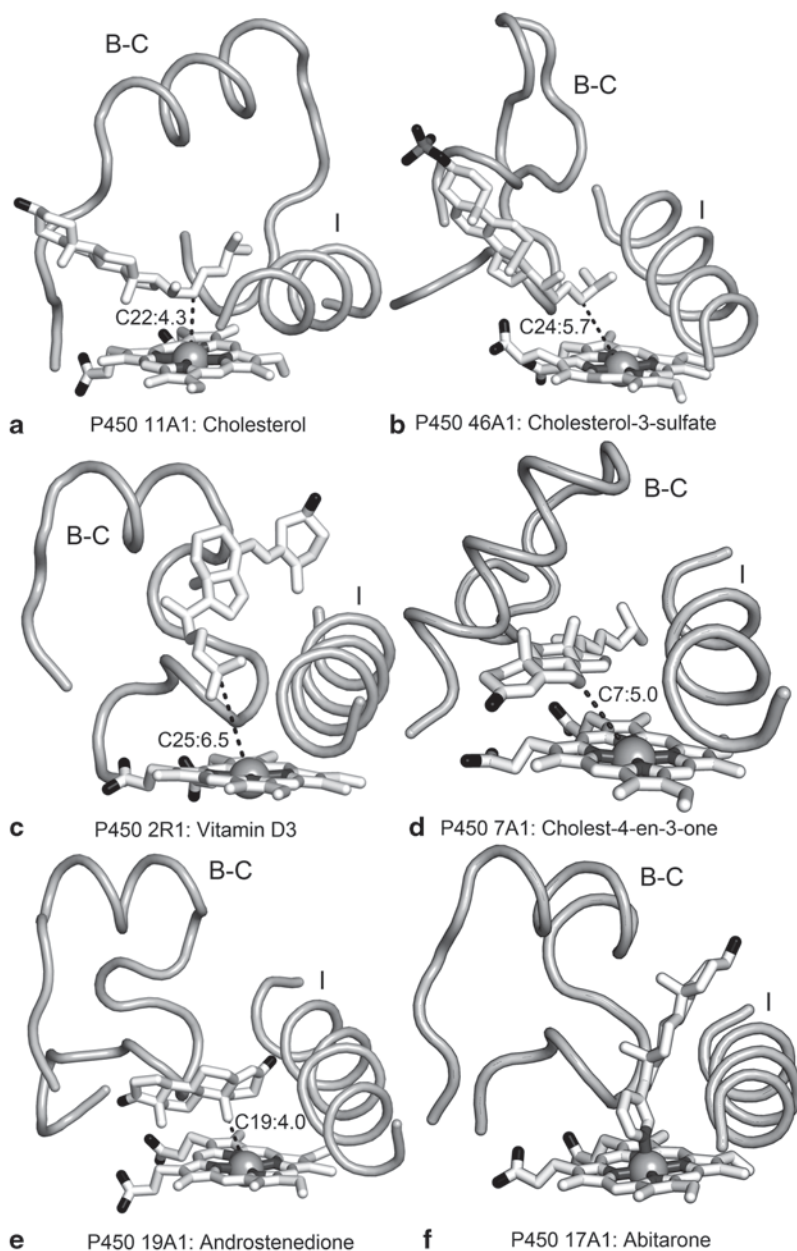


Fig. 1.18 Substrate and inhibitor binding to human P450s that catalyze key steps in steroid metabolism. The substrates, inhibitor, and heme are shown as stick figures with the heme iron depicted as a *sphere*. Nitrogen and oxygen atoms are colored *light gray* and *black*, respectively. The *dotted lines* represent the distance from the heme iron for

sites of metabolism labeled with the identity of the site of metabolism and the distance. The CYP17A1 inhibitor abiraterone binds directly to the heme iron. For reference, a portion of helix I and the helix B–C loop are shown. The topology and length of the helix B–C loops exhibit significant variation between proteins

hydroxycholesterol and 22*R*,20*R*-dihydroxycholesterol, indicate that the tetracyclic sterol moiety is positioned similarly to that of cholesterol in each case, with changes in the dihedral angles of the side chain positioning the appropriate site of metabolism close to the heme iron. The structure of CYP46A1 [103] indicates that cholesterol sulfate binds similarly, but the aliphatic side chain is positioned with C24 closest to the heme iron, Fig. 1.18b. In contrast, an X-ray crystal structure of P450 2R1 [104] reveals that the sterol moiety of vitamin D₃ is located under helix G near helices I and B' with the site of metabolism, C25, positioned closest to the heme iron, Fig. 1.18c.

Other steroid biosynthetic enzymes catalyze reactions that modify the rigid tetracyclic steroid ring system. Three enzymes, P450s 7A1, 7B1, and 39A1, insert an oxygen atom into the 7 α C–H bond to produce 7 α -hydroxylated intermediates in the formation of bile acids. A structure of P450 7A1 with the cholesterol analog, cholest-4-ene-3-one (PDB code 3SN5), indicates that the 7 α C–H bond is positioned closest to the heme iron and that the plane of the sterol ring is parallel to the plane of the heme, Fig. 1.18d. The aliphatic side-chain passes out of the substrate-binding cavity between helix I and the helix B'–C loop. Structures of P450s 19A1 [105] and 11B1 [71] also place the tetracyclic steroid ring system of androst-4-ene-3,20-dione and 21-hydroxyprogesterone in a similar location, but with the C19 methyl group, Fig. 1.18e, and the 11 β C–H bond, respectively, oriented toward the heme iron. P450 19A1 catalyzes three successive oxidations of the 19-methyl group with the product rearranging to produce formic acid and the unsaturated A ring of the estrogen, estrone.

Other reactions catalyzed by steroid biosynthetic enzymes target the ends of the steroid ring system. The structure of the adrenal 21-hydroxylase [106] with 17 α -hydroxyprogesterone bound reveals that the tetracyclic steroid is oriented almost perpendicular to the plane of the heme with the 17 β -side chain positioned near the heme iron. P450 17A1, which catalyzes the 17 α -hydroxylation of progesterone and cleavage of the 17 β -side chain of the pregnenolone to form androstenedione, has been crystallized with abiraterone [107] in the active site, Fig. 1.18f.

Abiraterone is used clinically for the treatment of prostate cancer via inhibition of androgen formation catalyzed by P450 17A1. The steroid moiety of abiraterone is oriented similarly to 17 α -hydroxyprogesterone in the P450 21A2 structure, with abiraterone coordinated to the heme iron through a heterocyclic nitrogen group. Structures of human CYP51A1 with inhibitors bound in the active site are also available to aid in the development of CYP51A1 inhibitors that will target these enzymes in pathogens without inhibiting the human enzyme [108, 109].

As is evident in Fig. 1.18, P450's have evolved to catalyze these reactions by positioning the substrates for site-selective metabolism, and, in doing so, different portions of the P450 structure are utilized for substrate binding. This, in turn, reflects differences in the sizes and properties of the amino acids that occupy the active site cavity as well as changes in protein conformation. Examples of these conformational differences are readily apparent when comparing the helix B–C loop regions depicted in the six panels of Fig. 1.18.

In contrast, P450s in families 1A, 2A, 2B, 2C, 2D, 2E, 2J, and 3A frequently contribute to the metabolic clearance of drugs and other xenobiotics. In the absence of evolutionary selection to optimize the binding of these compounds, many xenobiotic substrates are likely to exhibit relatively poor fits in P450 active sites and several isoenergetic binding poses may be possible, as suggested by the formation of multiple metabolites. Reaction rates are likely to reflect probabilities for binding to specific enzymes, relative reactivity of potential sites of reaction, and probabilities for placement of the sites of reaction near the oxene intermediate, leading to uncoupling, multiple metabolites and poor catalytic efficiencies. Fortunately, the enzymes that catalyze these reactions exhibit significant active site diversity that provides protection from a wide range of structurally diverse xenobiotics.

Family 1 and 3 enzymes exhibit very different active-site cavities. The enzymes in family 1 typically metabolize polynuclear aromatic hydrocarbons, and the structures of human CYP1A1 [110], 1A2 [64], and 1B1 [111] exhibit narrow active-site cavities that complement the size and

planarity of polynuclear aromatic hydrocarbons, as illustrated for CYP1A2 in Fig. 1.19a. These narrow active-site cavities are reinforced by a kink in helix F, which directs a portion of helix F and helix F' between the active site and the N-terminal domain. This is likely to add rigidity to the narrow active site cavity. In contrast, CYP3A4 exhibits a large and open active site cavity (Fig. 1.19b) with a much larger exposure of the heme surface to substrates than seen in other xenobiotic metabolizing enzymes [62, 112]. This difference underlies the capacity of 3A4 to catalyze oxygenation of the steroids at carbons 6 or 7 in the center of the ring system as seen for steroidogenic CYP7A1 in Fig. 1.18. CYP3A4 is

also unusual because helix F is short and does not cross above the active site. As a result, the active site can expand and contract by the flexible motion of the long connector between helix F and F' and changes in the positions of helices F' and G' [113]. The active-site cavities of human family 2 P450s range from small for P450s 2E1 [114, 115], 2A6 [116] Fig. 1.19c, 2A13 [117], and 2B6 [89, 90] to large for 2C8 [63], Fig. 1.2C9 [118, 119], 2C19 [120], and 2D6 [75, 121], and they can vary due to conformational changes associated with ligand access and binding [45]. As such, these enzymes contribute diverse capacities for xenobiotic metabolism.

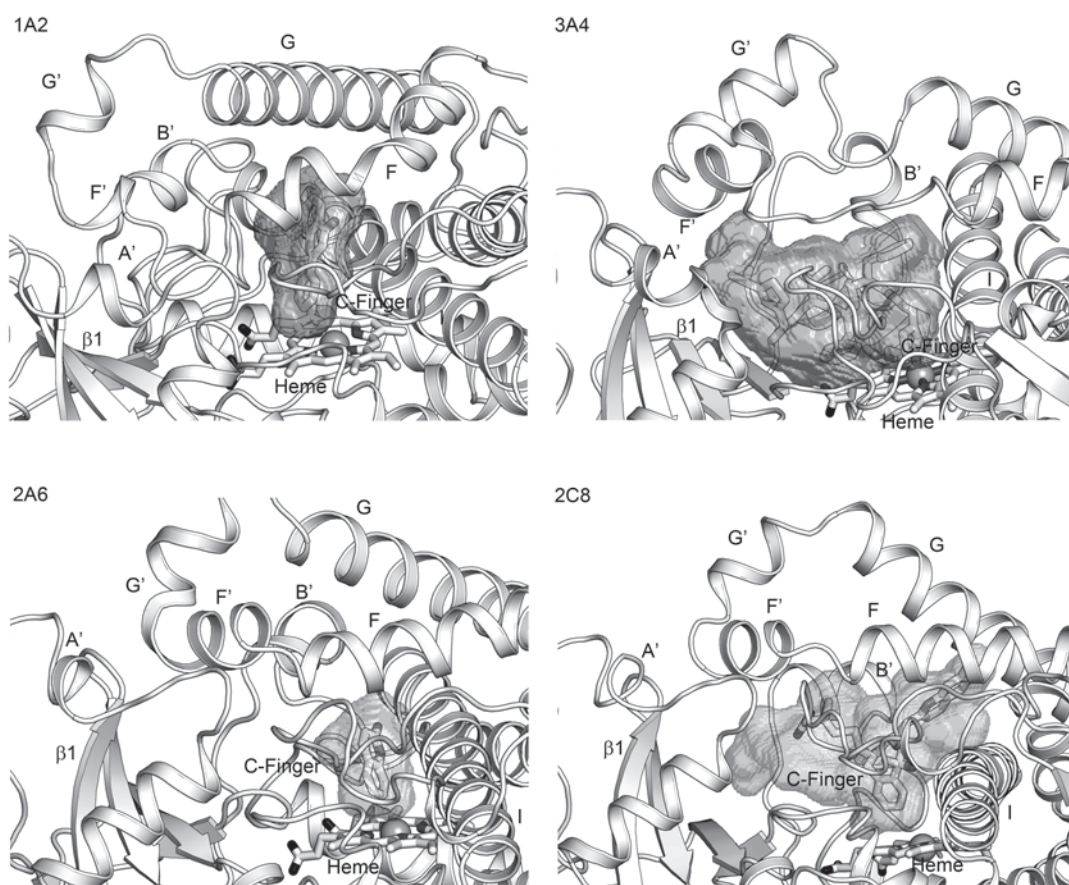


Fig. 1.19 Portions of the structures of the complex of CYP1A2 with α -naphthoflavone (PDB:2HI4), CYP3A4 with ritonavir (PDB:3NXU), CYP2A6 with coumarin (PDB:1Z10), and CYP2C8 with montelukast (PDB:2NNI) are shown as cartoons displaying secondary structures.

The heme and ligands are depicted as stick figures with the heme iron shown as a *sphere*. The surfaces of the active-site cavities were calculated using VOIDOO [157] and rendered as a transparent surface. Nitrogen and oxygen atoms are colored *light gray* and *black*, respectively

1.8 Electron Transfer Complexes

P450s do not operate alone but must form a complex with a redox partner for electron transfer. Protein redox complexes, including those involving P450s, are designed not to be very tight or long-lived. A complex that is too tight will have a slow dissociation rate, which precludes rapid turnover. Nature thus must strike a balance between specificity, affinity, and high turnover. Such complexes have proven quite difficult to crystallize, which is why there are very few protein–protein redox complexes in the PDB and, to date, there are only three crystal structures of a P450 complexed with a redox partner.

The first structure of a redox complex to be solved was that between the heme and FMN domains of P450BM3. Although P450BM3 is a bacterial enzyme, P450BM3 is more closely related in sequence, structure, activity, and redox partner to microsomal P450s than to other bacterial P450s. The unique feature of P450BM3 is that the diflavin P450 reductase is linked to the C-terminal end of the heme domain, thus giving a catalytically self-sufficient enzyme. Crystals were obtained by removing the FAD domain [122]. The structure (Fig. 1.20) shows

that the FMN domain docks on the proximal surface of the P450, which was expected, based on complementary electrostatic surfaces and mutagenesis studies. The linker connecting the heme and FMN domains had been proteolyzed during crystallization, thus raising the possibility that the structure is an artifact of crystallization. Further experiments were carried out to test the functional validity of the model. Residues found at the interface were probed by mutagenesis [123]. Replacing Leu104 of P450BM3 with a Cys (Fig. 1.20) at the interface should not alter binding or electron transfer because replacing Leu with a smaller side chain should not cause any steric problems in forming the proper complex. However, covalent modification of the mutant Cys104 side chain with a large fluorophore should interfere with electron transfer. For these studies, laser flash photolysis was used wherein a laser flash photoreduced a potent reductant, deazariboflavin, which in turn reduces the FMN in the complex. The reduced FMN semiquinone then reduces the P450 heme. As predicted, mutation of Leu104 to Cys had no effect, while chemical modification of Cys104 dramatically decreased the FMN-to-heme electron transfer rate, thus

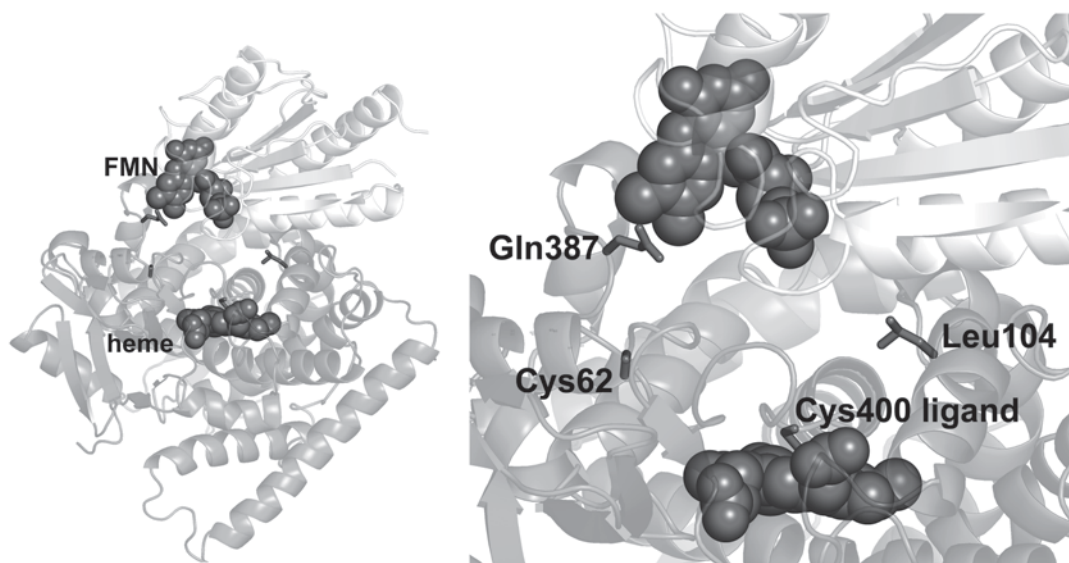


Fig. 1.20 Crystal structure of the P450BM3 electron-transfer complex (PDB: 1BVY) [122]. The closest contact at the interface is between Gln387 in the heme domain and the FMN

implicating Leu104 as an important residue in forming the proper electron transfer complex.

A second prediction from the P450BM3 electron-transfer complex structure that can be tested is the electron transfer path. The heme–FMN domain interface is shown in Fig. 1.20. The closest point of contact between the two domains places the FMN about 4 Å from the peptide backbone of Gln387. The peptide chain from Gln387 to the heme ligand, Cys400, could constitute an electron transfer path. To test this hypothesis, Gln387 was converted to Cys and modified with (4-bromomethyl-4'-methylbipyridine) [bis(bipyridine)]ruthenium(II) [124]. The covalently attached Ru(II) is photoreduced, and the rate of reduction of the heme Fe(III) to Fe(II) by the photo-generated Ru(I) was followed. The same experiment was carried out with Ru(II) attached to Cys62. Both Cys62 and Cys387 are about the same distance from the heme, but electron transfer from Cys60-Ru(II) must make “through-space” jumps, while there is a continuous covalent connection between Cys386-Ru(II) and the heme ligand, Cys400. In the case of Cys387-Ru(II), the heme iron was reduced at a rate of $4.6 \times 10^5 \text{ s}^{-1}$, while Cys60-Ru(II) did not

reduce the heme iron. These results indicate that if the crystal structure of P450BM3 electron-transfer complex is functionally relevant, then the electron-transfer reaction can readily proceed along the direct point of contact between the FMN and heme domain.

The structure of the complex formed between adrenodoxin (Adx) and P45011A1, which converts cholesterol to pregnenolone, also has been solved. The crystal structure of the complex was solved by fusing adrenodoxin to the N-terminal end of CYP11A1 [70]. Although a good part of the Adx was disordered and not visible in electron-density maps, the interface with CYP11A1 was well defined (Fig. 1.21). The interface is dominated by electrostatic interactions and those residues involved are consistent with mutagenesis and chemical modifications studies [125–127]. A comparison between the free enzyme [69] and the enzyme complexed with Adx are essentially identical, so Adx binding does not result in any significant structural change.

The most recent structure to be determined is the P450cam–Pdx complex crystal [128, 129] and NMR structures [128]. The P450cam–Pdx complex has received considerable attention es-

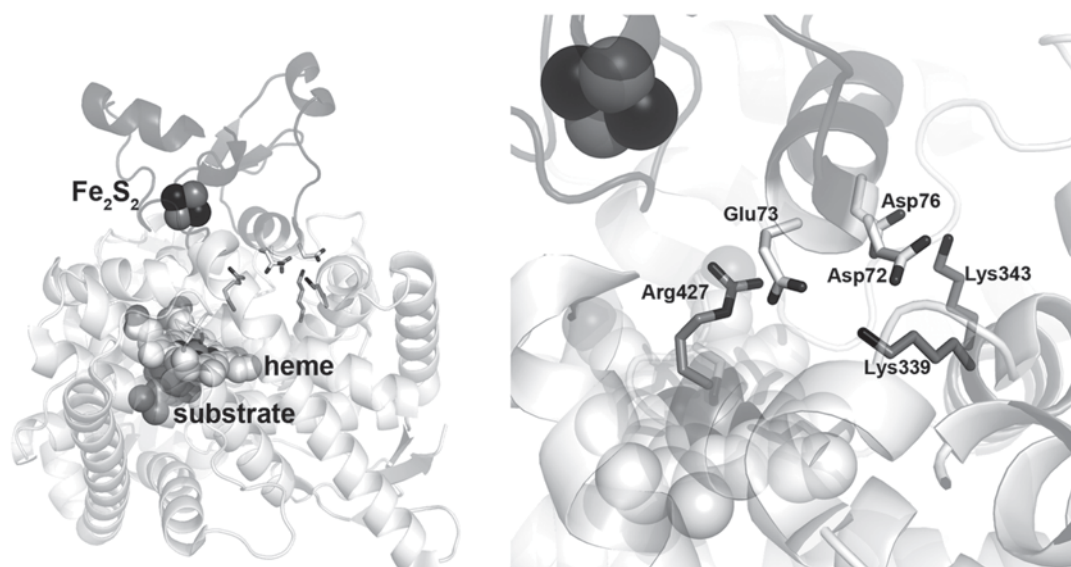


Fig. 1.21 Crystal structure of the complex formed between CYP11A1 and adrenodoxin (Adx; PDB: 3N9Y) [70]. Only part of the Adx is visible in electron-density

maps. The interface is dominated by ionic interactions. Adx binding does not result in any major structural change in CYP11A1

pecially since it was established some time ago that P450cam is not only very selective for Pdx but Pdx also plays an effector role by inducing structural changes required for electron transfer and O₂ activation [130–132]. Prior to the recent crystal structure of the P450cam–Pdx complex, Pochapsky et al. developed a model of the P450cam–Pdx complex using NMR and molecular modeling [133] that is supported by mutagenesis data [134–138]. A wealth of spectral data shows that when Pdx binds on the proximal side of the heme, spectral changes ensue that are associated with the opposite distal substrate-binding pocket. These changes include resonance Raman [139], infrared [138, 140], and NMR [141–143]. NMR studies [144–146] showed that Pdx binding results in changes in the B', C, F, and G helices that are well removed from where Pdx binds (Fig. 1.22). The B' helix provides key contacts with the substrate, while large movements of the F and G helices are the main features of the open/close transition [82]. Pdx binding to oxy-P450cam decreases the stability of the oxy complex 150-fold [147], while oxidized Pdx shifts oxidized P450cam to the low-spin state [148]. All these observations point to significant structural changes in P450cam when Pdx binds.

The crystal structure of the P450–Pdx complex [128, 129] shows that P450cam adopts the open conformation, which is consistent with previous spectroscopic studies. The structure of the reduced form of the complex has four P450–Pdx molecules in the asymmetric unit and in three of these, the product, hydroxycamphor, is bound [129]. This means that the open form in the complex is active in O₂ activation and hydroxylation. Interactions at the interface are consistent with earlier NMR studies [145] and mutagenesis data [43, 137, 138, 149–153]. Pdx_{Asp38} interacts with P450cam_{Arg112} (Fig. 1.22), which requires little movement in either protein in the vicinity of the ion pair. However, interactions involving Pdx_{Trp106}, which has been known for some time to be a critical residue [131], require movement of the C helix (Fig. 1.22). In effect, the C helix moves “up” about 2–3 Å in order to form nonpolar and H-bonding interactions with Pdx_{Trp106}. This motion of the C helix is coupled to movements in the B', I, F, and G helices, all of which are involved with substrate access or direct contacts with both substrates, camphor and O₂. This motion results in a large movement of the F and G helices and the F/G loop, which effectively opens the active site to bulk solvent. This open conformation is

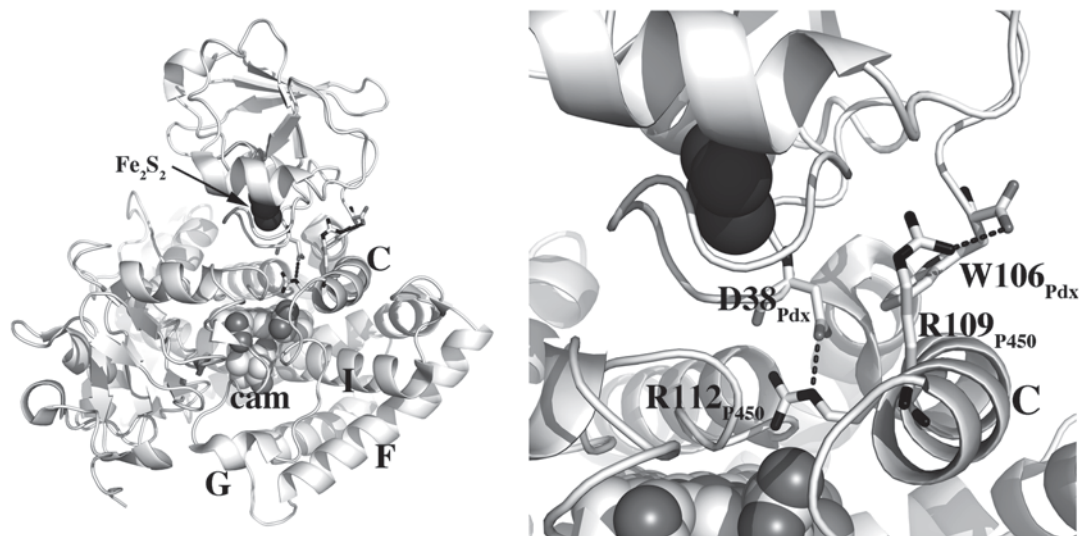


Fig. 1.22 Structure of the P450cam–Pdx complex (PDB: 4JX1) [129]. A key interaction is between Pdx_{Trp106} and the C helix in P450cam. The C helix moves “up” in order

to optimize interactions with Pdx_{Trp106}. This motion is coupled to an opening of the active site access channel on the opposite side of the protein (F/G helical region)

the same as observed by Lee et al. [82] The main difference is that in the structure solved by Lee et al. [82] the B' helix is disordered, while in a complex with Pdx the entire P450cam is highly ordered and the key interactions between camphor and the local environment remain, by and large, unchanged from the closed conformation. The main driving force for the conformational change appears to be Pdx_{Trp106}, which could not form tight interactions with P450cam without the structural switch.

The central question is why such Pdx-induced changes are important for activity. A possibly important part of the Pdx-induced structural change centers on the I helix near the O₂-binding site. The switch in the I helix in going from the closed to open state results in opening of the I helix similar to what happens when O₂ binds (Fig. 1.5). The closed to oxy-complex opening of the I helix is about midway between the extremes of the closed to fully open switch. This opening of the I helix is required to enable the catalytic waters to move into place for proton transfer to dioxygen [31, 33]. Thus, Pdx binding helps to stabilize the more oxy-like conformation of the I helix. However, the oxy-P450cam structure probably does not represent the final active state since Pdx binding perturbs the oxy-P450cam spectrum and results

in a 150-fold destabilization of the oxy complex [147]. It has been argued that Pdx “pushes” the oxy complex more toward the active form that is probably the more open conformation. Pdx also alters the electronic properties of the thiolate ligand [147, 148], which could be due to a shortening of the peptide NH-thiolate H-bond observed in the P450cam–Pdx crystal structure.

Another large change that occurs when Pdx binds involves Asp251. Asp251 is part of the I helix and is usually Asp or Glu in many other P450s. Asp251 is essential for activity in P450cam [154], P450cin [155], and CYP101D1 [88]. The Asp251Asn mutant in P450cam exhibits a two-orders-of-magnitude decrease in activity, yet remains tightly coupled [154]. That is, nearly all the electrons funneled into the P450cam mutant are utilized for substrate hydroxylation and not the wasteful production of water or peroxide. This mutant also exhibits a kinetic solvent isotope effect of 10 compared to 1.8 for wild-type P450cam [32]. This strongly implicates Asp251 as being intimately involved with the proper delivery of protons to dioxygen required for heterolytic cleavage of the O–O bond. The problem with this view, however, is that Asp251 is tied up with Arg187 and Lys178 in two strong ion pairs (Fig. 1.23). However, in the Pdx complex,

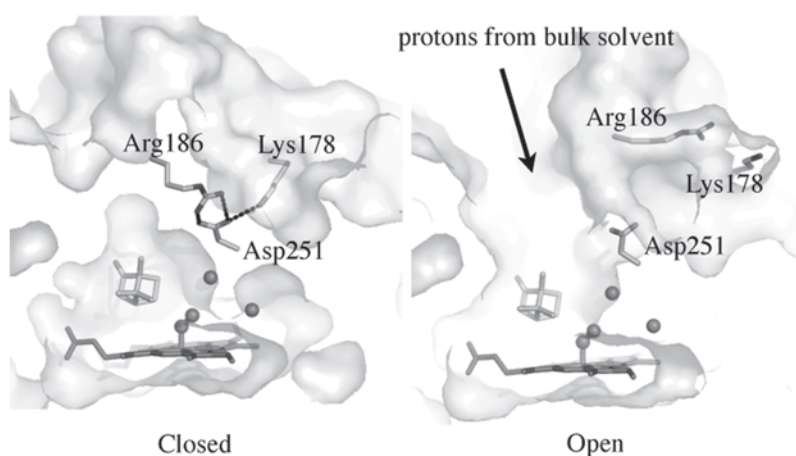


Fig. 1.23 The region around Asp251 in P450cam with and without Pdx bound. In the Pdx-free closed state, Asp251 is tied up in strong ion pairs with Arg186 and Lys178. When Pdx binds these ionic interactions are bro-

ken, thereby releasing Asp251 for its role in shuttling solvent protons to the iron-linked O₂ molecule required for O–O bond cleavage and thus, O₂ activation

these ion pairs are broken, which frees Asp251 to serve its proposed role in shuttling protons from bulk solvent into the active site. It thus appears that an important part of Pdx binding may be to “arm” the proton delivery machinery required for proton-coupled electron transfer.

The next obvious question is whether or not this sort of redox partner-mediated conformational change required for activity is a general property of all P450s or is limited to P450cam. The weight of the evidence so far indicates that P450cam may be an outlier. A number of P450s are known to be supported by nonphysiological redox partners and some redox partners, such as P450 reductase, service a large number of P450s. The only structural comparisons that can be made to address this question are the P450cam–Pdx and CYP11A1–Adx complexes [69]. CYP11A1 does not change to the open form in the complex but remains closed [69, 70]. However, Asp290 (corresponds to Asp251 in P450cam) is not tied up in ion pairs and is exposed to bulk solvent. Hence, no structural changes are required to free Asp290 for catalysis, although it has yet to be established if Asp290 is essential for CYP11A1 catalysis. Given that Nature has so many P450s, it is doubtful that P450cam is the only P450 where selective redox partner binding coupled with conformational selection is required for activity. It should only be a matter of time before similar P450s are uncovered and analyzed in depth. Just as interesting a question is the biological basis for such control. What is the evolutionary advantage, if any, of P450cam exhibiting such specificity, while very closely related P450s do not?

1.9 Conclusion

The large increase in P450 crystal structures over the past few years is due in large part to technological advances in protein expression and purification. Just as important are the increasing genome databases which now makes it relatively easy to “discover” new P450s. The sophistication of user-friendly crystallization robots, software, and synchrotron data collection has opened up crystallography to the nonexpert which also has

been a major contributor to the ever-expanding number of structures deposited in the protein database. In fact, the field is now at the stage where expression, purification, characterization, and crystal structure determination can outpace functional and biological studies. Many structures now are being solved before one knows much about function. We thus must start using structural information to guide functional and biological studies. This could be particularly important with orphan P450s that will continue to increase in number as more and more P450s are discovered in new and interesting places. Such advances coupled with powerful computational resources that can be used for molecular modeling and in silico screening of potential substrates can significantly contribute to a better understanding of function. Recent advances in defining various conformational states also is quite important since which conformational state one uses for virtual screening of substrate/inhibitors is obviously quite important. Now, however, we have a better idea on the various conformational states available to P450s which will further sharpen predictive computational tools. We thus anticipate that P450 structural biology will continue to move quickly but that much less time and energy will be devoted to the actual structure determination and instead, will be focused on function.

Acknowledgments TLP would like to thank members of the UCI P450 group, Dipanwita Batabyal, Huiying Li, Irina Sevrioukova, and Sarvind Tripathi, as well as NIH grant GM32688. EFJ would like to thank his colleagues at TSRI, Mei Hsu, Ying Fan, and C. David Stout, as well as the support of NIH Grant GM031001.

References

1. Poulos TL, Finzel BC, Gunsalus IC, Wagner GC, Kraut J (1985) The 2.6-Å crystal structure of *Pseudomonas putida* cytochrome P-450. *J Biol Chem* 260:16122–16130
2. Poulos TL, Finzel BC, Howard AJ (1987) High-resolution crystal structure of cytochrome P450cam. *J Mol Biol* 195:687–700
3. Ravichandran KG, Boddupalli SS, Haseremann CA, Peterson JA, Deisenhofer J (1993) Crystal structure of hemoprotein domain of P450BM-3, a prototype for microsomal P450's. *Science* 261:731–736

4. Shimizu H, Park SY, Shiro Y, Adachi S (2002) X-ray structure of nitric oxide reductase (cytochrome P450nor) at atomic resolution. *Acta Crystallogr D Biol Crystallogr* 58:81–89
5. Shoun H, Sudo Y, Seto Y, Beppu T (1983) Purification and properties of a cytochrome P-450 of a fungus, *Fusarium oxysporum*. *J Biochem* 94:1219–1229
6. Chiang CW, Yeh HC, Wang LH, Chan NL (2006) Crystal structure of the human prostacyclin synthase. *J Mol Biol* 364:266–274
7. Hecker M, Ullrich V (1989) On the mechanism of prostacyclin and thromboxane A2 biosynthesis. *J Biol Chem* 264:141–150
8. Li L, Chang Z, Pan Z, Fu ZQ, Wang X (2008) Modes of heme binding and substrate access for cytochrome P450 CYP74A revealed by crystal structures of allene oxide synthase. *Proc Natl Acad Sci U S A* 105:13883–13888
9. Brash AR (2009) Mechanistic aspects of CYP74 allene oxide synthases and related cytochrome P450 enzymes. *Phytochemistry* 70:1522–1531
10. Song WC, Brash AR (1991) Purification of an allene oxide synthase and identification of the enzyme as a cytochrome P-450. *Science* 253:781–784
11. Lee DS, Nioche P, Hamberg M, Raman CS (2008) Structural insights into the evolutionary paths of oxygen-lipin biosynthetic enzymes. *Nature* 455:363–368
12. Lee DS, Yamada A, Sugimoto H, Matsunaga I, Ogura H, Ichihara K, Adachi S, Park SY, Shiro Y (2003) Substrate recognition and molecular mechanism of fatty acid hydroxylation by cytochrome P450 from *Bacillus subtilis*. Crystallographic, spectroscopic, and mutational studies. *J Biol Chem* 278:9761–9767
13. Belcher J, McLean KJ, Matthews S, Woodward LS, Fisher K, Rigby SEJ, Nelson DR, Potts D, Baynham MT, Parker DA, Leys D, Munro AW (2014) Structure and biochemical properties of the alkene producing cytochrome P450 OleTJE (CYP152L1) from the *Jeotgalicoccus* sp. 8456 bacterium. *J Biol Chem* 289:6535–6550
14. Sundaramoorthy M, Terner J, Poulos TL (1995) The crystal structure of chloroperoxidase: a heme peroxidase–cytochrome P450 functional hybrid. *Structure* 3:1367–1377
15. Crane BR, Arvai AS, Ghosh DK, Wu C, Getzoff ED, Stuehr DJ, Tainer JA (1998) Structure of nitric oxide synthase oxygenase dimer with pterin and substrate. *Science* 279:2121–2126
16. Fischmann TO, Hruza A, Niu XD, Fossetta JD, Lunn CA, Dolphin E, Prongay AJ, Reichert P, Lundell DJ, Narula SK, Weber PC (1999) Structural characterization of nitric oxide synthase isoforms reveals striking active-site conservation. *Nat Struct Biol* 6:233–242
17. Raman CS, Li H, Martasek P, Kral V, Masters BS, Poulos TL (1998) Crystal structure of constitutive endothelial nitric oxide synthase: a paradigm for pterin function involving a novel metal center. *Cell* 95:939–950
18. Adman E, Watenpaugh KD, Jensen LH (1975) NH—S hydrogen bonds in *Peptococcus aerogenes* ferredoxin, *Clostridium pasteurianum* rubredoxin, and *Chromatium* high potential iron protein. *Proc Natl Acad Sci U S A* 72:4854–4858
19. Ueyama N, Nishikawa N, Yamada Y, Okamura T, Nakamura A (1996) Cytochrome P-450 model (porphyrinato)(thiolatio)iron(III) complexes with and double NH-S hydrogen bonds. *J Am Chem Soc* 118:1286–1287
20. Ueyama N, Terakawa T, Nakata M, Nakamura A (1983) Positive shift of redox potential of $[\text{Fe}^2\text{S}_4(\text{Z-cys-Gly-Ala-OMe})_4]^{2-}$ in dichloromethane. *J Am Chem Soc* 105:7098–7102
21. Poulos TL, Finzel BC (1984) Heme enzyme structure and function. In: Mearn MT (ed) *Peptide and protein reviews*. Marcel Dekker, New York, pp 115–171
22. Doeff MA, Sweigart DA, O'Brien P (1983) Hydrogen bonding from coordinated imidazole in ferric porphyrin complexes. Effect on the iron(III)/iron(II) reduction potential. *Inorg Chem* 22:851–852
23. Banci L, Bertini I, Pease EA, Tien M, Turano P (1992) ^1H NMR investigation of manganese peroxidase from *Phanerochaete chrysosporium*. A comparison with other peroxidases. *Biochemistry* 31:10009–10017
24. Chang CK, Traylor TG (1973) Proximal base influence on the binding of oxygen and carbon monoxide to heme. *J Am Chem Soc* 95:8477–8479
25. Nappa M, Valentine JS, Snyder PA (1977) Imidazolate complexes of ferric porphyrins. *J Am Chem Soc* 99:5799–5800
26. Valentine JS, Sheridan RP, Allen LC, Kahn PC (1979) Coupling between oxidation state and hydrogen bond conformation in heme proteins. *Proc Natl Acad Sci U S A* 76:1009–1013
27. Cupp-Vickery JR, Poulos TL (1995) Structure of cytochrome P450eryF involved in erythromycin biosynthesis. *Nat Struct Biol* 2:144–153
28. Meharena YT, Li H, Hawkes DB, Pearson AG, De Voss J, Poulos TL (2004) Crystal structure of P450cin in a complex with its substrate, 1,8-cineole, a close structural homologue to D-camphor, the substrate for P450cam. *Biochemistry* 43:9487–9494
29. Benson DE, Suslick KS, Sligar SG (1997) Reduced oxy intermediate observed in D251N cytochrome P450cam. *Biochemistry* 36:5104–5107
30. Denisov IG, Makris TM, Sligar SG, Schlichting I (2005) Structure and chemistry of cytochrome P450. *Chem Rev* 105:2253–2277
31. Schlichting I, Berendzen J, Chu K, Stock AM, Maves SA, Benson DE, Sweet RM, Ringe D, Petsko GA, Sligar SG (2000) The catalytic pathway of cytochrome p450cam at atomic resolution. *Science* 287:1615–1622
32. Vidakovic M, Sligar SG, Li H, Poulos TL (1998) Understanding the role of the essential Asp251 in cytochrome P450cam using site-directed mutagenesis, crystallography, and kinetic solvent isotope effect. *Biochemistry* 37:9211–9219
33. Nagano S, Poulos TL (2005) Crystallographic study on the dioxygen complex of wild-type and mutant cytochrome P450cam. Implications for the dioxygen

- activation mechanism. *J Biol Chem* 280:31659–31663
34. Nagano S, Cupp-Vickery JR, Poulos TL (2005) Crystal structures of the ferrous dioxygen complex of wild-type cytochrome P450eryF and its mutants, A245S and A245T: investigation of the proton transfer system in P450eryF. *J Biol Chem* 280:22102–22107
 35. Cupp-Vickery JR, Han O, Hutchinson CR, Poulos TL (1996) Substrate-assisted catalysis in cytochrome P450eryF. *Nat Struct Biol* 3:632–637
 36. Omura T, Ito A (1991) Biosynthesis and intracellular sorting of mitochondrial forms of cytochrome P450. *Methods Enzymol* 206:75–81
 37. Sakaguchi M, Omura T (1993) Topology and biogenesis of microsomal cytochrome P-450s. In: Ruckpaul K, Rein H (eds) *Medicinal implications in cytochrome P-450 catalyzed biotransformations*. Akademie, Berlin, pp 59–73
 38. White SH, Ladokhin AS, Jayasinghe S, Hristova K (2001) How membranes shape protein structure. *J Biol Chem* 276:32395–32398
 39. Andersen OS, Koeppe RE (2007) Bilayer thickness and membrane protein function: an energetic perspective. *Annu Rev Biophys Biomol Struct* 36:107–130
 40. Von Wachenfeldt C, Richardson TH, Cosme J, Johnson EF (1997) Microsomal P450 2C3 is expressed as a soluble dimer in *Escherichia coli* following modifications of its N-terminus. *Arch Biochem Biophys* 339:107–114
 41. Cosme J, Johnson EF (2000) Engineering microsomal cytochrome P450 2C5 to be a soluble, monomeric enzyme. Mutations that alter aggregation, phospholipid dependence of catalysis, and membrane binding. *J Biol Chem* 275:2545–2553
 42. Andersen JF, Hutchinson CR (1992) Characterization of *Saccharopolyspora erythraea* cytochrome P-450 genes and enzymes, including 6-deoxyerythronolide B hydroxylase. *J Bacteriol* 174:725–735
 43. Koga H, Sagara Y, Yaoi T, Tsujimura M, Nakamura K, Sekimizu K, Makino R, Shimada H, Ishimura Y, Yura K, et al (1993) Essential role of the Arg112 residue of cytochrome P450cam for electron transfer from reduced putidaredoxin. *FEBS Lett* 331:109–113
 44. Pernecky SJ, Larson JR, Philpot RM, Coon MJ (1993) Expression of truncated forms of liver microsomal P450 cytochromes 2B4 and 2E1 in *Escherichia coli*: influence of NH 2-terminal region on localization in cytosol and membranes. *Proc Natl Acad Sci U S A* 90:2651–2655
 45. Johnson EF, Stout CD (2013) Structural diversity of eukaryotic membrane cytochrome P450s. *J Biol Chem* 288:17082–17090
 46. Ghosh D, Griswold J, Erman M, Pangborn W (2009) Structural basis for androgen specificity and oestrogen synthesis in human aromatase. *Nature* 457:219–223
 47. Lo J, Di NG, Griswold J, Egbuta C, Jiang W, Gilardi G, Ghosh D (2013) Structural basis for the functional roles of critical residues in human cytochrome P450 aromatase. *Biochemistry* 52:5821–5829
 48. Yamamoto K, Gildenberg M, Ahuja S, Im SC, Pearcy P, Waskell L, Ramamoorthy A (2013) Probing the transmembrane structure and topology of microsomal cytochrome-P450 by solid-state NMR on temperature-resistant bicelles. *Sci Rep* 3:2556
 49. Monk BC, Tomasiak TM, Keniya MV, Huschmann FU, Tyndall JD, O'Connell J, Cannon RD, McDonald JG, Rodriguez A, Finer-Moore JS, Stroud RM (2014) Architecture of a single membrane spanning cytochrome P450 suggests constraints that orient the catalytic domain relative to a bilayer. *Proc Natl Acad Sci U S A* 111:3865–3870
 50. Williams PA, Cosme J, Sridhar V, Johnson EF, McRee DE (2000) The crystallographic structure of a mammalian microsomal cytochrome P450 monooxygenase: structural adaptations for membrane binding and functional diversity. *Mol Cell* 5:121–132
 51. Williams PA, Cosme J, Sridhar V, Johnson EF, McRee DE (2000) Microsomal cytochrome P450 2C5: comparison to microbial P450s and unique features. *J Inorg Biochem* 81:183–190
 52. Denisov IG, Shih AY, Sligar SG (2012) Structural differences between soluble and membrane bound cytochrome P450s. *J Inorg Biochem* 108:150–158
 53. De Lemos-Chiarandini C, Frey AB, Sabatini DD, Kreibich G (1987) Determination of the membrane topology of the phenobarbital-inducible rat liver cytochrome P-450 isoenzyme PB-4 using site-specific antibodies. *J Cell Biol* 104:209–219
 54. Von Wachenfeldt C, Johnson EF (1995) Structures of eukaryotic cytochrome P450 enzymes. In: Ortiz de Montellano PR (ed) *Cytochrome P450: structure, mechanism, and biochemistry*, 2nd edn. Plenum Press, New York, pp 183–244
 55. Bayburt TH, Sligar SG (2002) Single-molecule height measurements on microsomal cytochrome P450 in nanometer-scale phospholipid bilayer disks. *Proc Natl Acad Sci U S A* 99:6725–6730
 56. Shank-Retzlaff ML, Raner GM, Coon MJ, Sligar SG (1998) Membrane topology of cytochrome P450 2B4 in langmuir-blodgett monolayers. *Arch Biochem Biophys* 359:82–88
 57. Cojocaru V, Balali-Mood K, Sansom MS, Wade RC (2011) Structure and dynamics of the membrane-bound cytochrome P450 2C9. *PLoS Comput Biol* 7:e1002152
 58. Berka K, Hendrychova T, Anzenbacher P, Otyepka M (2011) Membrane position of ibuprofen agrees with suggested access path entrance to cytochrome P450 2C9 active site. *J Phys Chem A* 115:11248–11255
 59. Berka K, Paloncova M, Anzenbacher P, Otyepka M (2013) Behavior of human cytochromes P450 on lipid membranes. *J Phys Chem B* 117:11556–11564
 60. Baylon JL, Lenov IL, Sligar SG, Tajkhorshid E (2013) Characterizing the membrane-bound state of cytochrome P450 3A4: structure, depth of insertion, and orientation. *J Am Chem Soc* 135:8542–8551
 61. Ohta Y, Kawato S, Tagashira H, Takemori S, Komimami S (1992) Dynamic structures of adrenocortical cytochrome P-450 in proteoliposomes and microsomes: protein rotation study. *Biochemistry* 31:12680–12687

62. Williams PA, Cosme J, Vinkovic DM, Ward A, Angove HC, Day PJ, Vonrhein C, Tickle IJ, Jhoti H (2004) Crystal structures of human cytochrome P450 3A4 bound to metyrapone and progesterone. *Science* 305:683–686
63. Schoch GA, Yano JK, Wester MR, Griffin KJ, Stout CD, Johnson EF (2004) Structure of human microsomal cytochrome P450 2C8. Evidence for a peripheral fatty acid binding site. *J Biol Chem* 279:9497–9503
64. Sansen S, Yano JK, Reynald RL, Schoch GA, Griffin KJ, Stout CD, Johnson EF (2007) Adaptations for the oxidation of polycyclic aromatic hydrocarbons exhibited by the structure of human P450 1A2. *J Biol Chem* 282:14348–14355
65. Ozalp C, Szczesna-Skorupa E, Kemper B (2006) Identification of membrane-contacting loops of the catalytic domain of cytochrome P450 2C2 by tryptophan fluorescence scanning. *Biochemistry* 45:4629–4637
66. Davydov DR (2011) Microsomal monooxygenase as a multienzyme system: the role of P450-P450 interactions. *Expert Opin Drug Metab Toxicol* 7:543–558
67. Szczesna-Skorupa E, Mallah B, Kemper B (2003) Fluorescence resonance energy transfer analysis of cytochromes P450 2C2 and 2E1 molecular interactions in living cells. *J Biol Chem* 278:31269–31276
68. Hu G, Johnson EF, Kemper B (2010) CYP2C8 exists as a dimer in natural membranes. *Drug Metab Dispos* 38:1976–1983
69. Mast N, Annalora AJ, Lodowski DT, Palczewski K, Stout CD, Pikuleva IA (2011) Structural basis for three-step sequential catalysis by the cholesterol side chain cleavage enzyme CYP11A1. *J Biol Chem* 286:5607–5613
70. Strushkevich N, MacKenzie F, Cherkesova T, Grabovec I, Usanov S, Park HW (2011) Structural basis for pregnenolone biosynthesis by the mitochondrial monooxygenase system. *Proc Natl Acad Sci U S A* 108:10139–10143
71. Strushkevich N, Gilep AA, Shen L, Arrowsmith CH, Edwards AM, Usanov SA, Park HW (2013) Structural insights into aldosterone synthase substrate specificity and targeted inhibition. *Mol Endocrinol* 27:315–324
72. Annalora AJ, Goodin DB, Hong WX, Zhang Q, Johnson EF, Stout CD (2010) The crystal structure of CYP24A1, a mitochondrial cytochrome P450 involved in vitamin D metabolism. *J Mol Biol* 396:441–451
73. Murtazina D, Puchkaev AV, Schein CH, Oezguen N, Braun W, Nanavati A, Pikuleva IA (2002) Membrane-protein interactions contribute to efficient 27-hydroxylation of cholesterol by mitochondrial cytochrome P450 27A1. *J Biol Chem* 277:37582–37589
74. Headlam MJ, Wilce MC, Tuckey RC (2003) The F-G loop region of cytochrome P450scc (CYP11A1) interacts with the phospholipid membrane. *Biochim Biophys Acta* 1617:96–108
75. Rowland P, Blaney FE, Smyth MG, Jones JJ, Leydon VR, Oxbrow AK, Lewis CJ, Tennant MG, Modi S, Eggleston DS, Chenery RJ, Bridges AM (2006) Crystal structure of human cytochrome P450 2D6. *J Biol Chem* 281:7614–7622
76. Nakayama K, Puchkaev A, Pikuleva IA (2001) Membrane binding and substrate access merge in cytochrome P450 7A1, a key enzyme in degradation of cholesterol. *J Biol Chem* 276:31459–31465
77. Poulos TL, Finzel BC, Howard AJ (1986) Crystal structure of substrate-free *Pseudomonas putida* cytochrome P450. *Biochemistry* 25:5314–5322
78. Li H, Poulos TL (1997) The structure of the cytochrome P450BM-3 haem domain complexed with the fatty acid substrate, palmitoleic acid. *Nat Struct Biol* 4:140–146
79. Haines DC, Tomchick DR, Machius M, Peterson JA (2001) Pivotal role of water in the mechanism of P450BM-3. *Biochemistry* 40:13456–13465
80. Li H, Poulos TL (1995) Modeling protein substrate interactions in the heme domain of cytochrome P450BM-3. *Acta Crystallogr D* 51:21–32
81. Paulsen MD, Ornstein RL (1995) Dramatic differences in the motions of the mouth of open and closed cytochrome P450BM-3 by molecular dynamics simulations. *Proteins* 21:237–243
82. Lee YT, Wilson RF, Rupniewski I, Goodin DB (2010) P450cam visits an open conformation in the absence of substrate. *Biochemistry* 49:3412–3419
83. Hays AM, Dunn AR, Chiu R, Gray HB, Stout CD, Goodin DB (2004) Conformational states of cytochrome P450cam revealed by trapping of synthetic molecular wires. *J Mol Biol* 344:455–469
84. Lee Y-T, Glazer EC, Wilson RF, Stout CD, Goodin DB (2011) Three clusters of conformational states in P450cam reveal a multistep pathway for closing of the substrate access channel. *Biochemistry* 50:693–703
85. Yang W, Bell SG, Wang H, Zhou W, Hoskins N, Dale A, Bartlam M, Wong L-L, Rao Z (2010) Molecular characterization of a class I P450 electron transfer system from *Novosphingobium aromaticivorans* DSM1(2444). *J Biol Chem* 285:27372–27384
86. Yang W, Bell SG, Wang H, Zhou W, Bartlam M, Wong L-L, Rao Z (2010) The structure of CYP101D2 unveils a potential path for substrate entry into the active site. *Biochem J* 433:85–93
87. Vohra S, Musgaard M, Bell S, Wong LL, Zhou W, Biggin PC (2013) The dynamics of camphor in the cytochrome P450 CYP101D2. *Protein Sci* 22:1218–1229
88. Batabyal D, Poulos TL (2013) Crystal structures and functional characterization of wild-type CYP101D1 and its active site mutants. *Biochemistry* 52:8898–8906
89. Gay SC, Shah MB, Talakad JC, Maekawa K, Roberts AG, Wilderman PR, Sun L, Yang JY, Huelga SC, Hong WX, Zhang Q, Stout CD, Halpert JR (2010) Crystal structure of a cytochrome P450 2B6 genetic variant in complex with the inhibitor 4-(4-chlorophenyl)imidazole at 2.0-Å resolution. *Mol Pharmacol* 77:529–538
90. Shah MB, Wilderman PR, Pascual J, Zhang Q, Stout CD, Halpert JR (2012) Conformational adaptation of human cytochrome P450 2B6 and rabbit cytochrome P450 2B4 revealed upon binding multiple amlodipine molecules. *Biochemistry* 18:7225–7238

91. Zhao Y, White MA, Muralidhara BK, Sun L, Halpert JR, Stout CD (2006) Structure of microsomal cytochrome P450 2B4 complexed with the antifungal drug bifonazole: insight into P450 conformational plasticity and membrane interaction. *J Biol Chem* 281:5973–5981
92. Scott EE, He YA, Wester MR, White MA, Chin CC, Halpert JR, Johnson EF, Stout CD (2003) An open conformation of mammalian cytochrome P450 2B4 at 1.6-Å resolution. *Proc Natl Acad Sci U S A* 100:13196–13201
93. Cojocaru V, Winn PJ, Wade RC (2007) The ins and outs of cytochrome P450s. *Biochim Biophys Acta* 1770:390–401
94. Modi S, Sutcliffe MJ, Primrose WU, Lian LY, Roberts GC (1996) The catalytic mechanism of cytochrome P450 BM3 involves a 6 Å movement of the bound substrate on reduction. *Nat Struct Biol* 3:414–417
95. Nagano S, Li H, Shimizu H, Nishida C, Ogura H, Ortiz de Montellano PR, Poulos TL (2003) Crystal structures of epothilone D-bound, epothilone B-bound, and substrate-free forms of cytochrome P450epoK. *J Biol Chem* 278:44886–44893
96. Bower S, Perkins JB, Yocum RR, Howitt CL, Rahaim P, Pero J (1996) Cloning, sequencing, and characterization of the *Bacillus subtilis* biotin biosynthetic operon. *J Bacteriol* 178:4122–4130
97. Cryle MJ, De Voss JJ (2004) Carbon-carbon bond cleavage by cytochrome p450(BioI)(CYP107H1). *Chem Commun (Camb)* 86–87
98. Cryle MJ, Matovic NJ, De Voss JJ (2003) Products of cytochrome P450(BioI) (CYP107H1)-catalyzed oxidation of fatty acids. *Org Lett* 5:3341–3344
99. Cryle MJ, Schlichting I (2008) Structural insights from a P450 carrier protein complex reveal how specificity is achieved in the P450(BioI) ACP complex. *Proc Natl Acad Sci U S A* 105:15696–15701
100. Zhao B, Lei L, Vassilyev DG, Lin X, Cane DE, Kelly SL, Yuan H, Lamb DC, Waterman MR (2009) Crystal structure of albaflavenone monooxygenase containing a moonlighting terpene synthase active site. *J Biol Chem* 284:36711–36719
101. Miller DJ, Allemann RK (2012) Sesquiterpene synthases: passive catalysts or active players? *Nat Prod Rep* 29:60–71
102. Akhtar M, Wright JN, Lee-Robichaud P (2011) A review of mechanistic studies on aromatase (CYP19) and 17 α -hydroxylase-17,20-lyase (CYP17) *J Steroid Biochem Mol Biol* 125:2–12
103. Mast N, White MA, Bjorkhem I, Johnson EF, Stout CD, Pikuleva IA (2008) Crystal structures of substrate-bound and substrate-free cytochrome P450 46A1, the principal cholesterol hydroxylase in the brain. *Proc Natl Acad Sci U S A* 105:9546–9551
104. Strushkevich N, Usanov SA, Plotnikov AN, Jones G, Park HW (2008) Structural analysis of CYP2R1 in complex with vitamin D₃. *J Mol Biol* 380:95–106
105. Ghosh D, Griswold J, Erman M, Pangborn W (2010) X-ray structure of human aromatase reveals an androgen-specific active site. *J Steroid Biochem Mol Biol* 118:197–202
106. Zhao B, Lei L, Kagawa N, Sundaramoorthy M, Banerjee S, Nagy LD, Guengerich FP, Waterman MR (2012) Three-dimensional structure of steroid 21-hydroxylase (cytochrome P450 21A2) with two substrates reveals locations of disease-associated variants. *J Biol Chem* 287:10613–10622
107. DeVore NM, Scott EE (2012) Structures of cytochrome P450 17A1 with prostate cancer drugs abiraterone and TOK-001. *Nature* 482:116–119
108. Strushkevich N, Usanov SA, Park HW (2010) Structural basis of human CYP51 inhibition by antifungal azoles. *J Mol Biol* 397:1067–1078
109. Lepesheva GI, Hargrove TY, Anderson S, Kleshchenko Y, Furtak V, Wawrzak Z, Villalta F, Waterman MR (2010) Structural insights into inhibition of sterol 14 α -demethylase in the human pathogen *Trypanosoma cruzi*. *J Biol Chem* 285:25582–25590
110. Walsh AA, Szklarz GD, Scott EE (2013) Human cytochrome P450 1A1 structure and utility in understanding drug and xenobiotic metabolism. *J Biol Chem* 288:12932–12943
111. Wang A, Savas U, Stout CD, Johnson EF (2011) Structural characterization of the complex between α -naphthoflavone and human cytochrome P450 1B1. *J Biol Chem* 286:5736–5743
112. Yano JK, Wester MR, Schoch GA, Griffin KJ, Stout CD, Johnson EF (2004) The structure of human microsomal cytochrome P450 3A4 determined by X-ray crystallography to 2.05-Å resolution. *J Biol Chem* 279:38091–38094
113. Ekroos M, Sjogren T (2006) Structural basis for ligand promiscuity in cytochrome P450 3A4. *Proc Natl Acad Sci U S A* 103:13682–13687
114. Porubsky PR, Meneely KM, Scott EE (2008) Structures of human cytochrome P450 2E1: insights into the binding of inhibitors and both small molecular weight and fatty acid substrates. *J Biol Chem* 283:33698–33707
115. Porubsky PR, Battaile KP, Scott EE (2010) Human cytochrome P450 2E1 structures with fatty acid analogs reveal a previously unobserved binding mode. *J Biol Chem* 285:22282–22290
116. Yano JK, Hsu MH, Griffin KJ, Stout CD, Johnson EF (2005) Structures of human microsomal cytochrome P450 2A6 complexed with coumarin and methoxsalen. *Nat Struct Mol Biol* 12:822–823
117. Smith BD, Sanders JL, Porubsky PR, Lushington GH, Stout CD, Scott EE (2007) Structure of the human lung cytochrome P450 2A13. *J Biol Chem* 282:17306–17313
118. Williams PA, Cosme J, Ward A, Angove HC, Matak VD, Jhoti H (2003) Crystal structure of human cytochrome P450 2C9 with bound warfarin. *Nature* 424:464–468
119. Wester MR, Yano JK, Schoch GA, Yang C, Griffin KJ, Stout CD, Johnson EF (2004) The structure of human microsomal cytochrome P450 2C9 com-

- plexed with flurbiprofen at 2.0 Å resolution. *J Biol Chem* 279:35630–35637
120. Reynald RL, Sansen S, Stout CD, Johnson EF (2012) Structural characterization of human cytochrome P450 2C19: active site differences between P450's 2C8, 2C9 and 2C19. *J Biol Chem* 287:44581–44591
121. Wang A, Savas U, Hsu MH, Stout CD, Johnson EF (2012) Crystal structure of human cytochrome P450 2D6 with prinomastat bound. *J Biol Chem* 287:10834–10843
122. Sevrioukova IF, Li H, Zhang H, Peterson JA, Poulos TL (1999) Structure of a cytochrome P450-redox partner electron-transfer complex. *Proc Natl Acad Sci U S A* 96:1863–1868
123. Sevrioukova IF, Hazzard JT, Tollin G, Poulos TL (1999) The FMN to heme electron transfer in cytochrome P450BM-3. Effect of chemical modification of cysteines engineered at the FMN-heme domain interaction site. *J Biol Chem* 274:36097–36106
124. Sevrioukova IF, Immoos CE, Poulos TL, Farmer P (2000) Electron transfer in the ruthenated heme domain of cytochrome P450BM-3. *Isr J Chem* 40:47–53
125. Adamovich TB, Pikuleva IA, Chashchin VL, Usanov SA (1989) Selective chemical modification of cytochrome P-450SCC lysine residues. Identification of lysines involved in the interaction with adrenodoxin. *Biochim Biophys Acta* 996:247–253
126. Coghlan VM, Vickery LE (1991) Site-specific mutations in human ferredoxin that affect binding to ferredoxin reductase and cytochrome P450sc. *J Biol Chem* 266:18606–18612
127. Wada A, Waterman MR (1992) Identification by site-directed mutagenesis of two lysine residues in cholesterol side-chain cleavage cytochrome P450 that are essential for adrenodoxin binding. *J Biol Chem* 267:22877–22882
128. Hiruma Y, Hass MA, Kikui Y, Liu WM, Olmez B, Skinner SP, Blok A, Kloosterman A, Koteishi H, Lohr F, Schwalbe H, Nojiri M, Ubbink M (2013) The structure of the cytochrome P450cam-putidaredoxin complex determined by paramagnetic NMR spectroscopy and crystallography. *J Mol Biol*. <http://www.ncbi.nlm.nih.gov/pubmed/23856620>
129. Tripathi S, Li H, Poulos TL (2013) Structural basis for effector control and redox partner recognition in cytochrome P450. *Science* 340:1227–1230
130. Lipscomb JD, Sligar SG, Namtvedt MJ, Gunsalus IC (1976) Autooxidation and hydroxylation reactions of oxygenated cytochrome P-450cam. *J Biol Chem* 251:1116–1124
131. Sligar SG, Debrunner PG, Lipscomb JD, Namtvedt MJ, Gunsalus IC (1974) A role of the putidaredoxin COOH-terminus in P-450cam (cytochrome m) hydroxylations. *Proc Natl Acad Sci U S A* 71:3906–3910
132. Tyson CA, Lipscomb JD, Gunsalus IC (1972) The role of putidaredoxin and P450 cam in methylene hydroxylation. *J Biol Chem* 247:5777–5784
133. Pochapsky TC, Lyons TA, Kazanis S, Arakaki T, Ratnaswamy G (1996) A structure-based model for cytochrome P450cam-putidaredoxin interactions. *Biochimie* 78:723–733
134. Geren L, Tuls J, O'Brien P, Millett F, Peterson JA (1986) The involvement of carboxylate groups of putidaredoxin in the reaction with putidaredoxin reductase. *J Biol Chem* 261:15491–15495
135. Imai M, Shimada H, Watanabe Y, Matsushimahiya Y, Makino R, Koga H, Horiuchi T, Ishimura Y (1989) Uncoupling of the cytochrome P-450cam monooxygenase reaction by a single mutation, threonine-252 to alanine or valine—a possible role of the hydroxy amino-acid in oxygen activation. *Proc Natl Acad Sci U S A* 86:7823–7827
136. Kuznetsov VY, Poulos TL, Sevrioukova IF (2006) Putidaredoxin-to-cytochrome P450cam electron transfer: differences between the two reductive steps required for catalysis. *Biochemistry* 45:11934–11944
137. Unno M, Shimada H, Toba Y, Makino R, Ishimura Y (1996) Role of Arg112 of cytochrome P450cam in the electron transfer from reduced putidaredoxin. Analyses with site-directed mutants. *J Biol Chem* 271:17869–17874
138. Shimada H, Nagano S, Hori H, Ishimura Y (2001) Putidaredoxin-cytochrome P450cam interaction. *J Inorg Biochem* 83:255–260
139. Unno M, Christian JF, Sjodin T, Benson DE, Macdonald ID, Sligar SG, Champion PM (2002) Complex formation of cytochrome P450cam with putidaredoxin. Evidence for protein-specific interactions involving the proximal thiolate ligand. *J Biol Chem* 277:2547–2553
140. Nagano S, Shimada H, Tarumi A, Hishiki T, Kimata-Arigo Y, Egawa T, Suematsu M, Park SY, Adachi S, Shiro Y, Ishimura Y (2003) Infrared spectroscopic and mutational studies on putidaredoxin-induced conformational changes in ferrous CO-P450cam. *Biochemistry* 42:14507–14514
141. Shiro Y, Iizuka T, Makino R, Ishimura Y, Morishima I (1989) N-15 NMR-Study on cyanide (C-15n) complex of cytochrome-P-450cam—Effects of D-camphor and putidaredoxin on the iron ligand structure. *J Am Chem Soc* 111:7707–7711
142. Tosha T, Yoshioka S, Ishimori K, Morishima I (2004) L358P mutation on cytochrome P450cam simulates structural changes upon putidaredoxin binding: the structural changes trigger electron transfer to oxy-P450cam from electron donors. *J Biol Chem* 279:42836–42843
143. Tosha T, Yoshioka S, Takahashi S, Ishimori K, Shimada H, Morishima I (2003) NMR study on the structural changes of cytochrome P450cam upon the complex formation with putidaredoxin. Functional significance of the putidaredoxin-induced structural changes. *J Biol Chem* 278:39809–39821
144. Pochapsky SS, Pochapsky TC, Wei JW (2003) A model for effector activity in a highly specific biological electron transfer complex: the cytochrome

- P450(cam)-putidaredoxin couple. *Biochemistry* 42:5649–5656
145. Zhang W, Pochapsky SS, Pochapsky TC, Jain NU (2008) Solution NMR structure of putidaredoxin-cytochrome P450cam complex via a combined residual dipolar coupling-spin labeling approach suggests a role for Trp106 of putidaredoxin in complex formation. *J Mol Biol* 384:349–363
 146. OuYang B, Pochapsky SS, Dang M, Pochapsky TC (2008) A functional proline switch in cytochrome P450cam. *Structure* 16:916–923
 147. Glascock MC, Ballou DP, Dawson JH (2005) Direct observation of a novel perturbed oxyferrous catalytic intermediate during reduced putidaredoxin-initiated turnover of cytochrome P-450-CAM: probing the effector role of putidaredoxin in catalysis. *J Biol Chem* 280:42134–42141
 148. Unno M, Christian JF, Benson DE, Gerber NC, SSligar SG, Champion PM (1997) Resonance Raman investigations of cytochrome P450cam complexed with putidaredoxin. *J Am Chem Soc* 119:6614–6620
 149. Davies MD, Qin L, Beck JL, Suslick KS, Koga H, Horiuchi T, SSligar SG (1990) Putidaredoxin reduction of cytochrome P-450cam—dependence of electron-transfer on the identity of putidaredoxins C-terminal amino-acid. *J Am Chem Soc* 112:7396–7398
 150. Davies MD, SSligar SG (1992) Genetic variants in the putidaredoxin-cytochrome P-450cam electron-transfer complex: identification of the residue responsible for redox-state-dependent conformers. *Biochemistry* 31:11383–11389
 151. Holden M, Mayhew M, Bunk D, Roitberg A, Vilker V (1997) Probing the interactions of putidaredoxin with redox partners in camphor P450 5-monooxygenase by mutagenesis of surface residues. *J Biol Chem* 272:21720–21725
 152. Pochapsky T, Lyons TA, Kazanis S, Arakaki T, Ratnaswamy G (1996) A structure-based model for cytochrome P450cam-putidaredoxin interactions. *Biochimie* 78:723–733
 153. Stayton PS, SSligar SG (1991) Structural microheterogeneity of a tryptophan residue required for efficient biological electron transfer between putidaredoxin and cytochrome P-450cam. *Biochemistry* 30:1845–1851
 154. Gerber NC, SSligar SG (1994) A role for Asp-251 in cytochrome P-450cam oxygen activation. *J Biol Chem* 269:4260–4266
 155. Stok JE, Yamada S, Farlow AJ, Slessor KE, De Voss JJ (2013) Cytochrome P450(cin) (CYP176A1) D241N: investigating the role of the conserved acid in the active site of cytochrome P450s. *Biochim Biophys Acta* 1834:688–696
 156. Bridges A, Gruenke L, Chang YT, Vakser IA, Loew G, Waskell L (1998) Identification of the binding site on cytochrome P450 2B4 for cytochrome b₅ and cytochrome P450 reductase. *J Biol Chem* 273:17036–17049
 157. Kleywegt GJ, Jones TA (1994) Detection, delineation, measurement and display of cavities in macromolecular structures. *Acta Crystallogr D Biol Crystallogr* 50:178–185